electronics

MDPI

Article

RETRACTED: Kinematic of the Position and Orientation Synchronization of the Posture of a *n* DoF Upper-Limb Exoskeleton with a Virtual Object in an Immersive Virtual Reality Environment

Deyby Huamanchahua *, Adriana Vargas-Martinez * and Ricardo Ramirez-Mendoza *

Tecnologico de Monterrey, School of Engineering and Sciences, Ave, Eugenio Garza Sada 2501, Monterrey 64849, Mexico

* Correspondence: deymihuca@hotmail.com (D.H.); adriana.vargas.mtz@tec.mx (A.V.-M.); ricardo.ramirez@tec.mx (R.R.-M.)

Abstract: Exoskeletons are an external structural mechanism with joints and links that work in tandem with the user, which increases, reinforces, or restores human performance. Virtual Reality can be used to produce environments, in which the intensity of practice and feedback on performance can be manipulated to provide tailored motor training. Will it be possible to combine both technologies and have them synchronized to reach better performance? This paper consists of the kinematics analysis for the position and orientation synchronization between an *n* DoF upper-limb exoskeleton pose and a projected object in an immersive virtual reality environment using a VR headset. To achieve this goal, the exoskeletal mechanism is analyzed using Euler angles and the Pieper technique to obtain the equations that lead to its orientation, forward, and inverse kinematic models. This paper extends the author's previous work by using an early stage upper-limb exoskeleton prototype for the synchronization process.

Keywords: upper-limb exoskeleton; immersive virtual reality; kinematics; pose synchronization

check for updates

Citation: Huamanchahua, D.; Vargas-Martinez, A.; Ramirez-Mendoza, R. RETRACTED: Kinematic of the Position and Orientation Synchronization of the Posture of a *n* DoF Upper-Limb Exoskeleton with a Virtual Object in an Immersive Virtual Reality Environment. *Electronics* **2021**, *10*, 1069. https://doi.org/10.3390/electronics10091069

Academic Editors: Christos P. Antonopoulos, Nikolaos Voros and Georgios Keramidas

Received: 19 March 2021
Accepted: 23 April 2021
Published: 30 April 2021
Retracted: 3 September 2024

Publisher's Note: MDPI stays neutral with regard to jurisdictional claims in published maps and institutional affiliations.

Copyright: © 2021 by the authors. Licensee MDPI, Basel, Switzerland. This article is an open access article distributed under the terms and conditions of the Creative Commons Attribution (CC BY) license (https://creativecommons.org/licenses/by/4.0/).

1. Introduction

Throughout history, men have created machines to enhance comfort or facilitate tasks by performing the most difficult, dangerous, and repetitive activities. The evolution of such artifacts has seen a particular boost of their human-machine interaction capabilities, leading to a crescent interest in human augmentation for both industrial and therapeutic applications.

In recent years, exoskeletal robots for upper or lower limbs have gained interest in the engineering community, which are designed to aid their users in activities such as rehabilitation, training, etc. These exoskeletal robots [1–3] which are commonly referred to as exoskeletons, power suits, man amplifiers, man magnifiers, or power assist systems, have been mainly studied for military or industrial use from the early 1960s. The recent technological advances that emerged in the last decade, including digital manufacturing and rapid prototyping, have boosted the development of these devices. Exoskeleton design requires careful attention to provide natural motion of the users without endangering their safety [4,5], which can be achieved by the application of biomimetic design methods [6].

One of the most rapidly growing fields of exoskeletons is rehabilitation [7–9], where the interaction between the human limb and the mechanism aids and augments the physical capacity of the subject. In this field, exoskeletons are known for improving the rehabilitation treatment, as well as the quality of life of patients suffering from neuromuscular disorders, such as stroke, spinal cord injury or muscular dystrophy [4,10–13]. Human upper-limb biomechanics represents one of the main challenges on exoskeleton design, where musculoskeletal systems allow multiple degrees of freedom (DoF) [14,15]. Various

RETRACTED

This paper has been retracted. A retraction notice was published on 3 September 2024 in *Electronics* **2024**, *13*, 3493. https://doi.org/10.3390/electronics13173493

configurations have been proposed for upper-limb exoskeleton systems [4,16–19]. However, many unsolved issues for natural interaction with the human body remain, especially in terms of kinematic singularities [20] and upper-limb biomechanics [21–23], e.g. shoulder elevation [24–26].

Furthermore, the physical coupling between an upper-limb exoskeleton and its human counterpart imposes many challenges when trying to create a successful integration of both systems [27–29]. For this reason, the ultimate goal of exoskeleton control is to increase the transparency of the human-robot mobility to minimize the interaction forces between pairs, in other words, the mechanism of the exoskeleton must coexist mimicking human biomechanics [30,31]. Upper-limb complexity lays in the number of DoF that is provided by their subsystems, where altogether, shoulder (3 DoF excluding scapular movement), elbow (1 DoF), and wrist (3 DoF), deliver a total of 7 DoF of spatial motion. Given the redundant nature of the arm, it is possible to perform multiple pose configurations to complete a task or movement, which is expressed with a mathematical model with no single solution [32–34]. Hence, to solve this model, it is necessary to understand the motor control mechanism of the human arm and select the most adequate solution for its biomechanics [4,35,36].

As mentioned earlier, one of the most common applications of exoskeletons is rehabilitation, which mainly focuses on restoring the independence of users with disabilities so that they can carry out their daily activities [37,38]. Rehabilitation therapies are implemented by specialists and depending on the degree of disability of the patient and the damaged part of the body. In recent years, virtual reality (VR) has been rapidly adapted for delivering therapies in a highly engaging way. This technology presents simulated information allowing individuals to experience and interact with or within three-dimensional virtual environments [39]. VR can be used to produce exercises in which intensity, frequency, motion amplitude, and feedback can be manipulated to provide tailored motor training [40,41]. Studies in computational neurosciences have demonstrated that motor learning tasks are better assimilated compared with traditional training [42]. It is known that therapists that have been attending patients for a long time do not perform their tasks optimally due to tiredness. Also, the lack of real-time data about the patient performance and improvements contribute to the non-optimal therapy development [43,44]. Previous works have shown evidence of the VR technologies efficacy in rehabilitation [45–48], enhancing therapies with diverse immersive technologies that allow the users to hear, see, perceive haptic feedback, and navigate in interactive environments. VR and exoskeletal systems have been used together to enhance functional exercising [49–51], however, these technologies have been scarcely studied in immersive environments.

The main objective of the paper is to present the kinematic analysis of pose synchronization between an n DoF upper-limb exoskeleton, and an immersive virtual object projected by virtual reality glasses. For the realization of the kinematic tests, a prototype 5 DoF upper-limb exoskeleton previously proposed in the literature [6] is used as an example. One of the secondary objectives, is the use of inverse kinematics, forward kinematics and orientation that allow determining the orientation and translation workspace [52], and the joint angles of the upper-limb exoskeleton and the virtual object. Another secondary objective is the use of Pieper's Technique to obtain the joint angles (γ_1, γ_2, γ_3, γ_4) by inverse kinematics [53–55] and the use of Euler's Parameters and Euler's Angles to obtain the position (P_X, P_Y, P_Z) and orientation (α, β, γ) parameters by forward kinematics and orientation [33,56–58]. Finally, the last secondary objective, is to obtain the MSE and SE to check and verify that the mathematical models obtained are correct.

For the realization of all the objectives, the methodology applied in this paper is as follows. First, the outline of the model of the position and orientation synchronization of the systems (upper-limb exoskeleton and virtual object) is presented, where the framework of the kinematic analysis of this work is introduced. Also, a description and kinematic analysis of the 5 DoF exoskeleton used for testing and the virtual object projected through virtual reality is performed, where the direct kinematics, orientation, and inverse kinematics for

RETRACTED

the systems are proposed. Pieper's technique, Euler's parameters, and Euler's angles were used to obtain the kinematic analysis. The first procedure performed is shown in Section 2. Secondly, numerical analysis and simulations of the mathematical models of the synchronization between the two systems were performed. Two numerical examples were applied to validate the mathematical models obtained in the kinematic analysis. Additionally, the workspace of the upper-limb exoskeleton was obtained to perform the simulations and obtain the value of the MSE and SE of all the mathematical models to verify and check that the values are correct. The second procedure performed is shown in Section 3. Finally, Section 4 presents the conclusions, the applicability of the proposal, and future lines of intervention through the results.

2. Position and Orientation Synchronization Modelling

This paper proposes the pairing of position and orientation of an n DoF open kinematic chain end-effector (e.g., an exoskeleton) and a virtual object. This synchronization is achieved when both end-effector and virtual object reference frames are coincident within each other. Furthermore, this development is done in a fully immersive VR environment.

Emphasis is placed on inverse kinematics to know the correct angles of the joints to be configured in the proper position and orientation. To achieve correct synchronization, the n DoF upper-limb exoskeleton must reach the virtual object with a single set of angles in the joints.

For synchronization in VR systems, there are two options on the global reference frame, and it depends on the system. First, many of the systems do not have a global reference frame (google cardboard, etc.) because the whole system moves so that the person cannot move around in the workspace, but can only orient themselves. The second, advanced VR systems (Oculus Rift, etc.) generate a workspace and the person can move inside of the space. Because of the synchronization, it was proposed that the person should move in the workspace, so the second option was chosen. Therefore, a fixed global frame of reference was placed outside the person's reference frame, which generated two workspaces: one of the opened-loop kinematic chain of the exoskeleton and the other of the virtual reality workspace.

For convenience for the readers, to illustrate this concept, consider the system shown in Figure 1 that is composed of a VR headset, an n DoF open kinematic chain, and a virtual object. Furthermore, vectors are represented by lower case lettering (e.g., $\vec{e}_S$). Cartesian coordinate reference frames are denoted by upper case lettering in bold italic type (e.g., F_V). The homogeneous transformation matrices [59] are represented by upper case lettering (e.g., E) and the translational displacement given by the position vector in the Figure 1 can be described by the following homogeneous transformation translation matrix to homogenize all the mathematical calculations.

For analysis purposes, a global reference frame is placed at the point F_G. The VR headset position and orientation are given by a local reference frame F_H, whose global position is given by vector $\vec{e}_G \in \mathbb{R}^{4x1}$ and are data that the VR system provides. The open kinematic chain is composed by n links whose local position and orientation are described by the homogeneous transformation matrix $E_{i=1,2,\ldots,n}$ and are given by a local reference frame F_0. Note that the position of the exoskeleton is anchored as a reference to the position of the headset and the local reference frame F_V is located at the end-effector, whose local position is described by the vector $\vec{e}_P \in \mathbb{R}^{4x1}$. Furthermore, a local reference frame F_M is located in a given point in the virtual object.

E_0 to $E_n \in \mathbb{R}^{4x4}$ are the homogeneous transformation matrices of the open kinematic chain, ${}^{G}_{n}E_T \in \mathbb{R}^{4x4}$ is the general homogeneous transformation matrix of the open kinematic chain end-effector, $\vec{e}_R \in \mathbb{R}^{4x1}$ is the local position vector from the VR glasses to local reference frame F_0 and the data obtained for this position vector will be made from actual measurements (constant), $\vec{e}_S \in \mathbb{R}^{4x1}$ is the local vector from the VR glasses to the virtual object, $M \in \mathbb{R}^{4x4}$ is the homogeneous matrix of the virtual object, $\vec{e}_Q \in \mathbb{R}^{4x1}$ is the global vector from the local reference frame F_0 to the virtual object reference frame F_M, $\vec{e}_{ER}$ is an

RETRACTED

"error" position vector between the virtual object reference frame F_M and the end-effector reference frame F_V, and $\vec{e}_M \in \mathbb{R}^{4x1}$ is the global vector from the global reference frame F_G to the virtual object reference frame F_M.

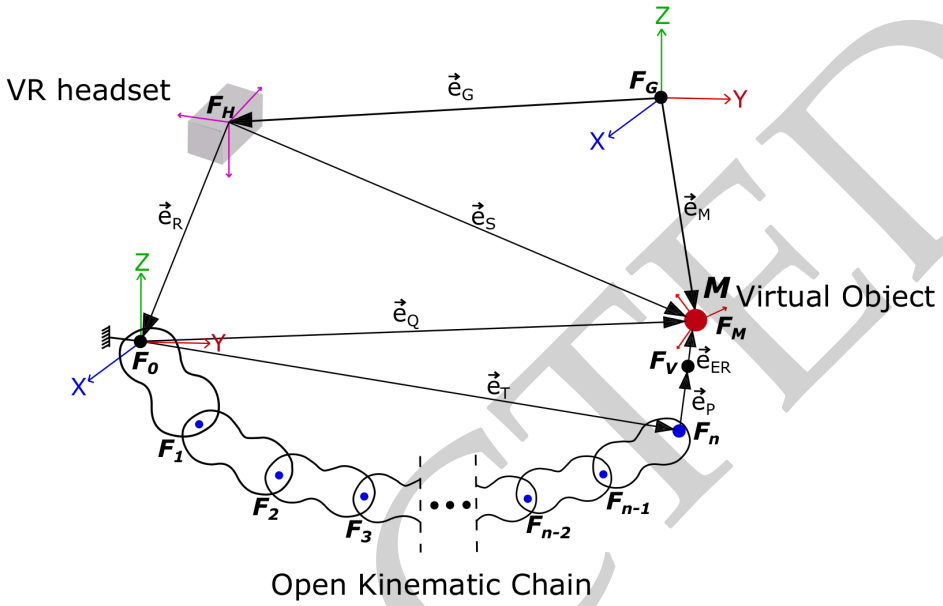


Figure 1. Kinematics Representation of n DoF Upper-Limb Exoskeleton with VR Glasses.

Inspecting the vector system in Figure 1, the following closed-loop equation is obtained:

$$\vec{e}_Q = {}^G_n E_T \,.\, \vec{e}_P + \vec{e}_{ER} \tag{1}$$

where,

$${}^G_n E_T = {}^G_1 E \,.\, {}^1_2 E \,.\, {}^2_3 E \,.\, \ldots . \,.\, {}^{n-1}_n E \tag{2}$$

Note that the position synchronization will occur when the following condition applies:

$$\vec{e}_{ER} = 0 \tag{3}$$

Which implies, from Equation (1), that:

$$\vec{e}_Q = {}^G_n E_T \,.\, \vec{e}_P \tag{4}$$

Namely, that the virtual object and the end-effector will have the same position. Furthermore, the two kinematics loops are established in the function of transformation homogeneous matrixes of the Figure 1. The first opened-loop equation (L_1) is the open kinematic chain of the exoskeleton from the global reference frame F_G to the virtual object reference frame F_M, where the transformation matrices E_G, E_R, and E_Q are from the vectors $\vec{e}_G$, $\vec{e}_R$, and $\vec{e}_Q$, respectively.

$$L_1 = E_G \,.\, E_R \,.\, E_Q \tag{5}$$

The second opened-loop equation (L_2) is the virtual object kinematic chain from the global reference frame F_G to the virtual object reference frame F_M, where the transformation matrices E_M, E_G and E_S are from the vectors $\vec{e}_M$, $\vec{e}_G$ and $\vec{e}_S$, respectively.

$$L_2 = E_M = E_G \,.\, E_S \tag{6}$$

Note that the position and orientation synchronization will occur when the following condition is set:

$$E_G \,.\, E_R \,.\, E_Q = E_G \,.\, E_S \tag{7}$$

RETRACTED

Hence, a position and orientation synchronization between an open kinematic chain and a virtual object will be achieved when Equation (7) is fulfilled.

2.1. Description of the 5 DoF Upper-Limb Exoskeleton

This paper will use a 5 DoF upper-limb exoskeleton that has been previously proposed in the literature [6] to demonstrate the concept of position and orientation synchronization. This section presents a description of the upper-limb exoskeleton and its kinematics analysis.

The prototype of the 5 DoF upper-limb exoskeleton has five rotational joints for providing mobility to the clavicle, shoulder, and elbow. Besides, the elbow joint is rotated 90° by mechanical design.

Consider the upper-limb exoskeleton that is presented in Figure 2, which is composed of an open kinematic chain whose links are serially connected to the base employing five revolute joints. The clavicle joint that is connected to the base is considered to be a passive DoF for this mechanism, while the joints j_1, j_2, and j_3 provide the 3 DoF of the shoulder, while joint j_4 provides 1 DoF for the elbow action.

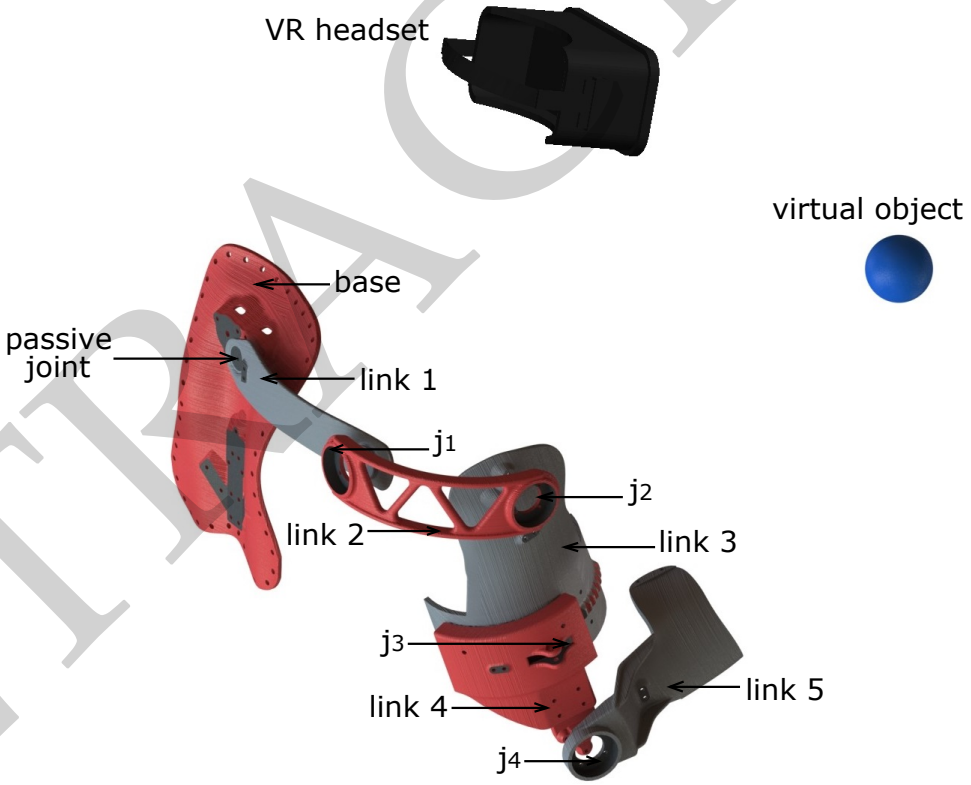


Figure 2. Description of the upper-limb exoskeleton CAD model.

Figure 3 shows the vector system of the 5 DoF upper-limb exoskeleton with a passive joint in the clavicle, which considers the ZXZ Euler convention, whose parameters are summarized in Table 1.

RETRACTED

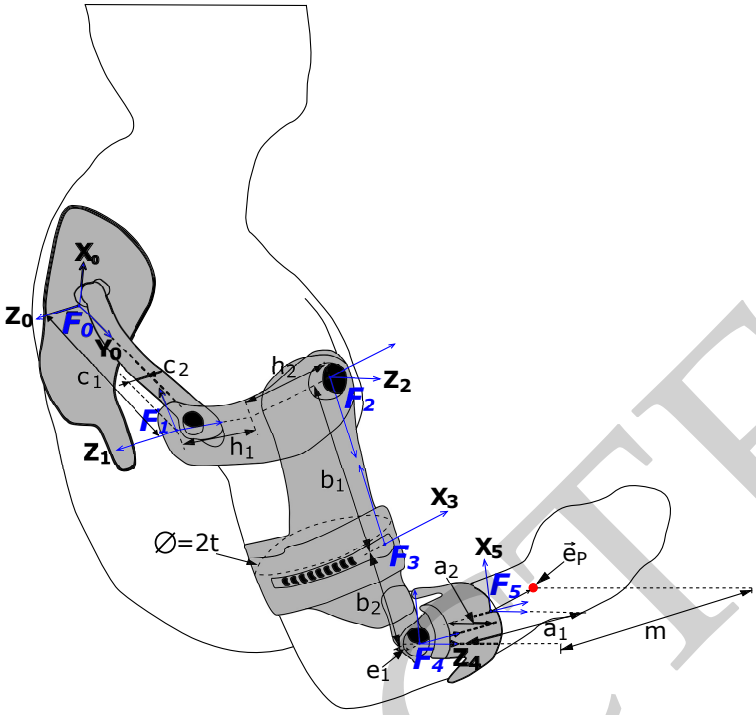


Figure 3. 5 DoF upper-limb exoskeleton vector system.

Table 1. ZXZ Euler parameters for the kinematic model of the upper-limb exoskeleton.

i	α	β	γ	d_x	d_y	d_z
1	0	$\pi/2$	γ_1	x_1	y_1	z_1
2	$-\pi/2$	$-\pi/2$	γ_2	h_1	0	$-h_2$
3	$\pi/2$	$-\pi/2$	γ_3	b_1	t $Sin\gamma_3$	t $Cos\gamma_3 - h_1$
4	0	$\pi/2$	γ_4 - $\pi/2$	0	$-e_1$	$-b_2$
5	$\pi/2$	$\pi/2$	0	a_1	0	$-a_2$

2.2. Forward Kinematics of the Upper-Limb Exoskeleton

The forward kinematics problem consists of finding a homogeneous transformation matrix that relates the angular position of the active joints to the position and orientation of the end-effector of the upper-limb exoskeleton [60–64]. The forward kinematics analysis of a 5 DoF exoskeleton was taken as a reference for illustration purposes in this work [6]. As the clavicle joint is considered passive, the forward kinematic, analysis will be for a 4 DoF exoskeleton.

Note, axes F_1, F_2, F_3, F_4 in Figure 3 represent the position of the mechanical joints, which are interconnected by links that compose the exoskeleton kinematic chain. The shoulder adduction/abduction axis is denoted as F_1. The F_2 axis describes the shoulder flexion/extension. To avoid self-constraining from joints, the F_3 axis is modelled as a circular sliding radial joint (with a $2t$ diameter) that is placed at the middle of the arm. The elbow flexion/extension axis is denoted as F_4, which is perpendicular to the shoulder rotational plane.

The homogeneous transformation matrix ${}^{G}_{5}E_T \in \mathbb{R}^{4x4}$ that expresses the upper-limb exoskeleton end-effector can be obtained by premultiplying the homogeneous transformation matrix E_i for $i = 1$ to $i = 5$.

$$ {}^{G}_{5}E_T(\gamma) = {}^{G}_{1}E(\gamma_1)\ {}^{1}_{2}E(\gamma_2)\ {}^{2}_{3}E(\gamma_3)\ {}^{3}_{4}E(\gamma_4)\ {}^{4}_{5}E(\gamma_5) \quad (8) $$

RETRACTED

Hence, the global position vector $\vec{e}_Q$ of a known point in the last local reference frame F_n is obtained as:

$$\vec{e}_Q = {}^{G}_{5}E_T(\gamma) \ . \ \vec{e}_P \tag{9}$$

The position vector $\vec{e}_P \in \mathbb{R}^{4x1}$ is a point in the middle of the forearm cross-section at an m distance (see Figure 3).

$$\vec{e}_P^T = \begin{bmatrix} 0 & a_1 - e_1 - t & m - a_1 & 1 \end{bmatrix} \tag{10}$$

Consider the ZXZ Euler parameters of Table 1 for obtaining the homogeneous matrix of each upper-limb exoskeleton chain. Where C and S denote Sine and Cosine, respectively. Substituting Equations (8) and (9) into Equation (10) and performing the matrix multiplications results in:

$$\vec{e}_Q^T = \begin{bmatrix} e_{Qx} & e_{Qy} & e_{Qz} & 1 \end{bmatrix} \tag{11}$$

$$e_{Qx} = x_1 + S\gamma_1 C\gamma_2 (b_1 + b_2) + m(S\gamma_1 C\gamma_2 C\gamma_4 - S\gamma_4 (S\gamma_1 S\gamma_2 C\gamma_3 + C\gamma_1 S\gamma_3)) \tag{12}$$

$$e_{Qy} = h_2 + y_1 + S\gamma_2 (b_1 + b_2) + m(S\gamma_2 C\gamma_4 + C\gamma_2 C\gamma_3 S\gamma_4) \tag{13}$$

$$e_{Qz} = z_1 - C\gamma_1 C\gamma_2 (b_1 + b_2) + m(-C\gamma_1 C\gamma_2 C\gamma_4 + S\gamma_4 (C\gamma_1 S\gamma_2 C\gamma_3 - S\gamma_1 S\gamma_3)) \tag{14}$$

To obtain the orientation of the upper-limb exoskeleton, the homogeneous transformation matrix $E_Q \in \mathbb{R}^{4x4}$ is defined:

$$E_Q = \begin{bmatrix} R(\alpha, \beta, \gamma)_{3x3} & e_Q(Px, Py, Pz)_{3x1} \\ 0^T & 1 \end{bmatrix} \tag{15}$$

Note that $R(\alpha, \beta, \gamma) \in \mathbb{R}^{3x3}$ is the rotation matrix and $e_Q(Px, Py, Pz) \in \mathbb{R}^{3x1}$ is the translation vector. Substituting Equations (8) and (10) into Equation (1), it is possible to determine the following elements of the equations of the rotation matrix $R(\alpha, \beta, \gamma)$ in Equation (15):

$$r_{11} = -C\gamma_4 (S\gamma_1 S\gamma_2 C\gamma_3 + C\gamma_1 S\gamma_3) - S\gamma_1 C\gamma_2 S\gamma_4 \tag{16}$$

$$r_{12} = C\gamma_1 C\gamma_3 - S\gamma_1 S\gamma_2 S\gamma_3 \tag{17}$$

$$r_{13} = S\gamma_1 C\gamma_2 C\gamma_4 - S\gamma_1 S\gamma_2 C\gamma_3 S\gamma_4 - C\gamma_1 S\gamma_3 S\gamma_4 \tag{18}$$

$$r_{21} = C\gamma_2 C\gamma_3 C\gamma_4 - S\gamma_2 S\gamma_4 \tag{19}$$

$$r_{22} = C\gamma_2 S\gamma_3 \tag{20}$$

$$r_{23} = S\gamma_2 C\gamma_4 + C\gamma_2 C\gamma_3 S\gamma_4 \tag{21}$$

$$r_{31} = -S\gamma_1 S\gamma_3 C\gamma_4 + C\gamma 1 S\gamma_2 C\gamma_3 C\gamma_4 + C\gamma_1 C\gamma_2 S\gamma_4 \tag{22}$$

$$r_{32} = S\gamma_1 C\gamma_3 + C\gamma_1 S\gamma_2 S\gamma_3 \tag{23}$$

$$r_{33} = -S\gamma_1 S\gamma_3 S\gamma_4 - C\gamma_1 C\gamma_2 C\gamma_4 + C\gamma_1 S\gamma_2 C\gamma_3 S\gamma_4 \tag{24}$$

Thus, the orientation of the end-effector is obtained by applying the successive ZXZ Euler angles convention, which is defined as:

$$R(\alpha, \beta, \gamma) = R_{Z,\alpha} \ . \ R_{X,\beta} \ . \ R_{Z,\gamma} = \begin{bmatrix} C\alpha C\gamma - S\alpha C\beta S\gamma & -C\alpha S\gamma - S\alpha C\beta C\gamma & S\alpha S\beta \\ S\alpha C\gamma + C\alpha C\beta S\gamma & -S\alpha S\gamma + C\alpha C\beta C\gamma & -C\alpha S\beta \\ S\beta S\gamma & S\beta C\gamma & C\beta \end{bmatrix} \tag{25}$$

RETRACTED

Note that α, β, γ can be determined for $\beta \in < 0\ ,\ \pi >$ from Equation (25) with the following equations.

$$\alpha = Atan2[r_{13}\ ,\ -r_{23}] \tag{26}$$

$$\beta = Atan2[\sqrt{r_{31}^2 + r_{32}^2}\ ,\ r_{33}] \tag{27}$$

$$\gamma = Atan2[r_{31}\ ,\ r_{32}] \tag{28}$$

Substituting Equations (18), (21)–(23) into Equations (26)–(28) results in:

$$\alpha = Atan2[\alpha_1, \alpha_2] \tag{29}$$

$$\beta = Atan2[\beta_1, \beta_2] \tag{30}$$

$$\gamma = Atan2[\gamma_1, \gamma_2] \tag{31}$$

where,

$$\alpha_1 = S\gamma_1 C\gamma_2 C\gamma_4 - S\gamma_1 S\gamma_2 C\gamma_3 S\gamma_4 - C\gamma_1 S\gamma_3 S\gamma_4$$

$$\alpha_2 = \ -S\gamma_2 C\gamma_4 - C\gamma_2 C\gamma_3 S\gamma_4$$

$$\beta_1 = \sqrt{(-S\gamma_1 S\gamma_3 C\gamma_4 + C\gamma_1 S\gamma_2 C\gamma_3 C\gamma_4 + C\gamma_1 C\gamma_2 S\gamma_4)^2 + (S\gamma_1 C\gamma_3 + C\gamma_1 S\gamma_2 S\gamma_3)^2}$$

$$\beta_2 = -S\gamma_1 S\gamma_3 C\gamma_4 - C\gamma_1 C\gamma_2 C\gamma_4 + C\gamma_1 S\gamma_2 C\gamma_3 S\gamma_4$$

$$\gamma_1 = -S\gamma_1 S\gamma_3 C\gamma_4 + C\gamma_1 S\gamma_2 C\gamma_3 C\gamma_4 + C\gamma_1 C\gamma_2 S\gamma_4$$

$$\gamma_2 = \ S\gamma_1 C\gamma_3 + C\gamma_1 S\gamma_2 S\gamma_3$$

2.3. Inverse Kinematics of the Upper-Limb Exoskeleton

The inverse kinematics problem consists of finding the configuration of the articular coordinates of the exoskeleton so that its end-effector is positioned and oriented according to a certain spatial location and pose [65–68].

Consider Equation (15), where n, o, and a denote the unit orientation vectors and the position vector $\vec{e}_P$ as a homogeneous transformation translation matrix $E_P \in \mathbb{R}^{4x4}$. Applying the inverse transformation operation (Pieper technique) to Equation (1) that consists in postmultiplying the homogeneous matrix E_i for $i = 1$ to $i = 5$ on the left-side in inverse form $(E_i)^{-1}$, namely:

$$E_Q = {}^{G}_{1}E(\gamma_1)\ {}^{1}_{2}E(\gamma_2)\ {}^{2}_{3}E(\gamma_3)\ {}^{3}_{4}E(\gamma_4)\ {}^{4}_{5}E(\gamma_5)\ E_P \tag{32}$$

$$({}^{G}_{1}E(\gamma_1))^{-1}\ E_Q = {}^{1}_{2}E(\gamma_2)\ {}^{2}_{3}E(\gamma_3)\ {}^{3}_{4}E(\gamma_4)\ {}^{4}_{5}E(\gamma_5)\ E_P \tag{33}$$

$$({}^{1}_{2}E(\gamma_2))^{-1}\ ({}^{0}_{1}E(\gamma_1))^{-1}\ E_Q = {}^{2}_{3}E(\gamma_3)\ {}^{3}_{4}E(\gamma_4)\ {}^{4}_{5}E(\gamma_5)\ E_P \tag{34}$$

$$({}^{2}_{3}E(\gamma_3))^{-1}\ ({}^{1}_{2}E(\gamma_2))^{-1}\ ({}^{G}_{1}E(\gamma_1))^{-1}\ E_Q = {}^{3}_{4}E(\gamma_4)\ {}^{4}_{5}E(\gamma_5)\ E_P \tag{35}$$

$$({}^{3}_{4}E(\gamma_4))^{-1}\ ({}^{2}_{3}E(\gamma_3))^{-1}\ ({}^{1}_{2}E(\gamma_2))^{-1}\ ({}^{G}_{1}E(\gamma_1))^{-1}\ E_Q = {}^{4}_{5}E(\gamma_5)\ E_P \tag{36}$$

$$({}^{4}_{5}E(\gamma_5))^{-1}\ ({}^{3}_{4}E(\gamma_4))^{-1}\ ({}^{2}_{3}E(\gamma_3))^{-1}\ ({}^{1}_{2}E(\gamma_2))^{-1}\ ({}^{G}_{1}E(\gamma_1))^{-1}\ E_Q = E_P \tag{37}$$

$$(E_P)^{-1}\ ({}^{4}_{5}E(\gamma_5))^{-1}\ ({}^{3}_{4}E(\gamma_4))^{-1}\ ({}^{2}_{3}E(\gamma_3))^{-1}\ ({}^{1}_{2}E(\gamma_2))^{-1}\ ({}^{G}_{1}E(\gamma_1))^{-1}\ E_Q = I \tag{38}$$

Table 2 shows the range of angles for each joint of the exoskeleton that is delimited to solve the inverse kinematics problem and obtain the mathematical models of each angle.

Table 2. Angle range per joint for the inverse kinematics solution.

Angle	γ_1	γ_2	γ_3	γ_4
Range	$< -180°, 180° >$	$< -90°, 90° >$	$< -90°, 90° >$	$< -180°, 180° >$

Six equations were obtained operations with matrices applying the Pieper technique, and these are observed in Equations (33)–(38). In the resolution of each matrix of each

RETRACTED

equation and, with the use of Table 2, 12 equations were extracted, resulting in a total of 72 equations. All of these were solved simultaneously to obtain the mathematical models of the active angular positions $\gamma_1, \gamma_2, \gamma_3, \gamma_4$:

$$\gamma_1 = Atan2[e_{Qx} - x_1 - a_X m \ , \ a_Z m - e_{Qz} + z_1] \tag{39}$$

$$\gamma_2 = Atan2[e_{Qy} - y_1 - h_2 - a_Y m \ , \ C\gamma_1(a_Z m - e_{Qz} + z_1) + S\gamma_1(e_{Qx} - x_1 - a_X m)] \tag{40}$$

$$\gamma_3 = Atan2[S\gamma_2(o_Z C\gamma_1 - o_X S\gamma_1) + o_Y C\gamma_2 \ , \ o_X C\gamma_1 + o_Z S\gamma_1] \tag{41}$$

$$\gamma_4 = Atan2[a_Y C\gamma_2 C\gamma_3 + S\gamma_2 C\gamma_3(a_Z C\gamma_1 - a_X S\gamma_1) - S\gamma_3(a_X C\gamma_1 - a_Z S\gamma_1 \ , \ n_Y C\gamma_2 C\gamma_3 + S\gamma_2 C\gamma_3(n_Z C\gamma_1 - n_X S\gamma_1 - S\gamma_3(n_Z S\gamma_1 + n_X C\gamma_1)] \tag{42}$$

The following section will present the kinematics of the virtual object, which will be used for the synchronization task.

2.4. Kinematics of the Virtual Object

Figure 4 shows the vector representation of the virtual object and the VR headset. Consider E_M a matrix that describes the position and orientation of the virtual object relative to the global frame F_G.

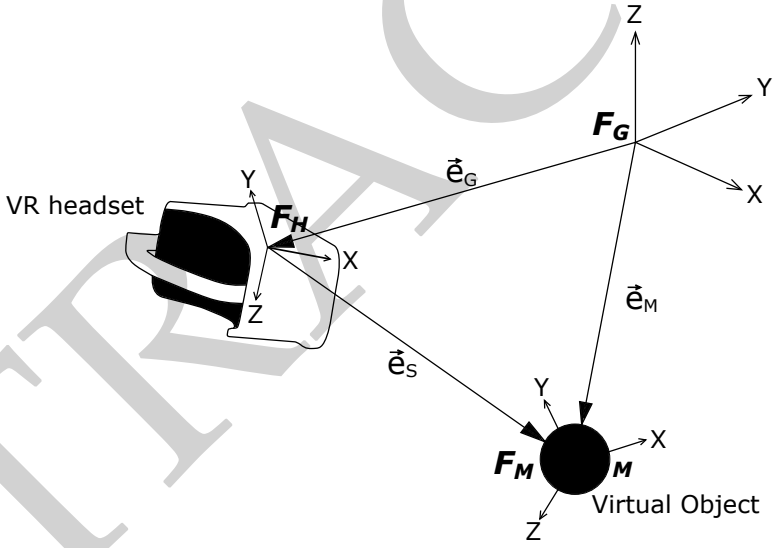


Figure 4. Vector Representation of the Virtual Object and the VR Headset.

Recalling Equation (6), the vectors $\vec{e}_S$ and $\vec{e}_G$ are considered to be a homogeneous transformation matrix (E_S) and homogeneous transformation translation matrix (E_G) respectively and can be expressed as follows:

$$E_M = E_G \ . \ E_S \tag{43}$$

The homogeneous transformation matrix E_M is:

$$E_M = \begin{bmatrix} 1 & 0 & 0 & E_{Gx} \\ 0 & 1 & 0 & E_{Gy} \\ 0 & 0 & 1 & E_{Gz} \\ 0 & 0 & 0 & 1 \end{bmatrix} . \begin{bmatrix} C\sigma C\psi - S\sigma C\phi S\psi & -C\sigma S\psi - S\sigma C\phi C\psi & S\sigma S\phi & E_{Sx} \\ S\sigma C\psi + C\sigma C\phi S\psi & -S\sigma S\psi + C\sigma C\phi C\psi & -C\sigma S\phi & E_{Sy} \\ S\phi S\psi & S\phi C\psi & C\phi & E_{Sz} \\ 0 & 0 & 0 & 1 \end{bmatrix} \tag{44}$$

RETRACTED

The matrix E_M that represents the position and orientation of the virtual object is obtained by premultiplying both matrices in Equation (43):

$$E_M = \begin{bmatrix} C\sigma C\psi - S\sigma C\phi S\psi & -C\sigma S\psi - S\sigma C\phi C\psi & S\sigma S\phi & E_{Gx} + E_{Sx} \\ S\sigma C\psi + C\sigma C\phi S\psi & -S\sigma S\psi + C\sigma C\phi C\psi & -C\sigma S\phi & E_{Gy} + E_{Sy} \\ S\phi S\psi & S\phi C\psi & C\phi & E_{Gz} + E_{Sz} \\ 0 & 0 & 0 & 1 \end{bmatrix} \quad (45)$$

This section determined the closed-loop equations for the position and orientation kinematics of a 5 DoF upper-limb exoskeleton and a virtual object. The following section will present numerical examples that illustrate the application of the position and orientation synchronization in robot kinematics.

3. Numerical Analysis and Simulation of the Mathematical Models of the Synchronization

This section presents a set of a numerical examples that are used to validate the closed-form equations that were obtained in previous sections for the kinematics analysis of the upper-limb exoskeleton and its pose synchronization with a virtual object.

3.1. Numerical Analysis of the Kinematic Models of the Upper-Limb Exoskeleton

The analytical results of the mathematical model of the upper-limb exoskeleton are validated in this paper by comparing the numerical examples with a computer simulation. Using the numerical examples, the kinematics and orientation equations will be validated. The errors of the equations will be obtained through the validation, resulting in errors approximately equal to zero to achieve synchronization. Table 3 shows the parameters of the initial configuration from the CAD mechanical model that was used for the numerical examples. Consider that, for reference purposes, the joint j_4 has an offset of 90°.

Table 3. Parameters of the initial position of the CAD mechanical design.

Parameter	x_1	y_1	z_1
Value (mm)	0	−14	0

Furthermore, Tables 4 and 5 show the dimensional parameters that were used for the numerical examples that were obtained from the CAD design of the upper-limb exoskeleton.

Table 4. Clavicle, Shoulder and Arm CAD mechanical design parameters.

Parameter	b_1	b_2	c_1	c_2	h_1	h_2	t
Value (mm)	161.19	91.79	172.55	21.89	114.38	101.23	83.13

Table 5. Forearm and Elbow CAD Mechanical Design Parameters.

Parameter	a_1	a_2	e_1	m
Value (mm)	136.01	38.50	13.70	200

3.1.1. First Numerical Analysis for the Angle Set

This comparison is developed by using a CAD upper-limb exoskeleton to analyze the trajectory of a point of a mechanical model of the system. The forward kinematics equations will be validated by using Table 6, which shows a set of values or configuration obtained from the CAD design, so a study of the movement was performed to validate the values. During the simulation, the mechanism is subjected to angular displacements in the rotation axes from a controlled position, beginning at time t = 0 s with an angular position where the four angles start at −110°, −50°, −40°, −80°; and, the ending position at time

RETRACTED

t = 60 s with an final angular position ends at 10°, 70°, 80°, and 40°. This angular position change is applied at a constant rate for every joint in both CAD and mathematical model simulation. These configurations of angles are used as starting angular positions for the numerical examples.

Table 6. Starting angular position for the numerical examples.

Angle	γ_1	γ_2	γ_3	γ_4
Range	$[-110°, 10°]$	$[-50°, 70°]$	$[-40°, 80°]$	$[-80°, 40°]$

1. Forward Kinematics of the Upper-Limb Exoskeleton

The position vector $P \in \mathbb{R}^{3x1}$ of the forward kinematics is obtained by Tables 3–6 and Equations (12)–(14). Using the equations of forward kinematics, the values of the final position are obtained for the angles that are defined in Table 6. When comparing to the values of the end position by the CAD mechanical model, both of the positions are identical. Figure 5a shows the graphical comparison of the final position between forward equations and CAD mechanical design. Furthermore, Figure 5b shows the Mean Square Error (MSE) of the final position that is obtained between the CAD mechanical and forward kinematics. Finally, Figure 5c shows the box plot representation of forward kinematics.

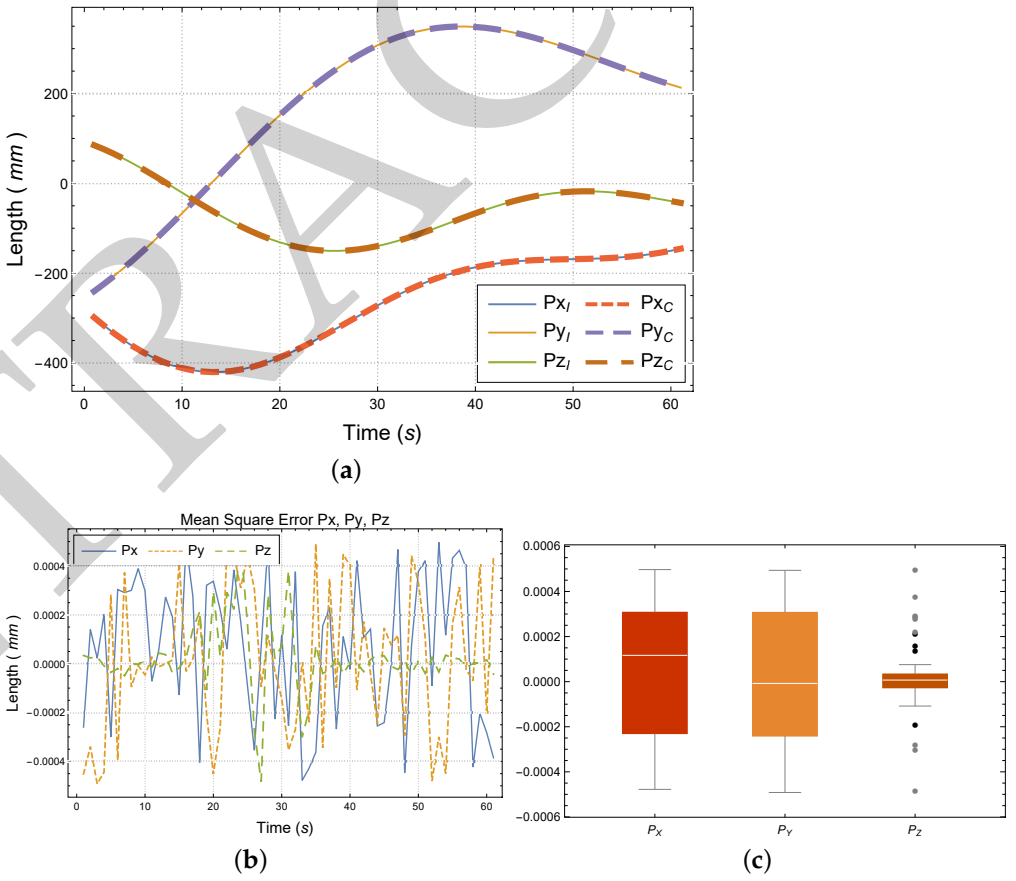


Figure 5. A comparison of the mathematical models of the forward kinematics. (**a**) Comparison of the position (P_X, P_Y, P_Z) between CAD mechanical design and forward kinematics equations. (**b**) Mean Square Error of the forward kinematics. (**c**) Box plot of the forward kinematics.

Table 7 shows the Mean Square Error and Standard Error of the resulting trajectories of the position. The results are approximately equal to zero, so the forward equations kinematics are correct.

RETRACTED

Table 7. Mean Squared Error (MSE) and Standard Error (SE) of the Forward Kinematics.

Position	P_X (mm)	P_Y (mm)	P_Z (mm)
MSE	6.91307×10^{-5}	1.34732×10^{-5}	2.04506×10^{-5}
SE	3.77342×10^{-5}	3.78417×10^{-5}	1.84893×10^{-5}

2. Orientation of the Upper-Limb Exoskeleton

The comparison of the orientation is developed by the rotation general equation and orientation equations. Using the Table 6 to validate the orientations equations by numerical examples obtained the values of α, β, γ. Substituting the values of the Table 6 in Equations (29)–(31) obtained the values of α, β, γ by orientation equations. Validating the orientation parameters, the general equation of rotation $R_i(\alpha, \beta, \gamma) \in \mathbb{R}^{3x3}$ in Equation (25) was used to compare both values of the angles. When comparing the results obtained using the equations of orientation and the general equation of rotation, the values obtained (α, β, γ) are identical. Furthermore, Figure 6a shows a graphical comparison using a set of values of the four angles, which are represented in Table 6. Figure 6b shows the Mean Square Error of the angle's orientation at approximately zero. Finally, Figure 6c shows the box plot representation of orientation.

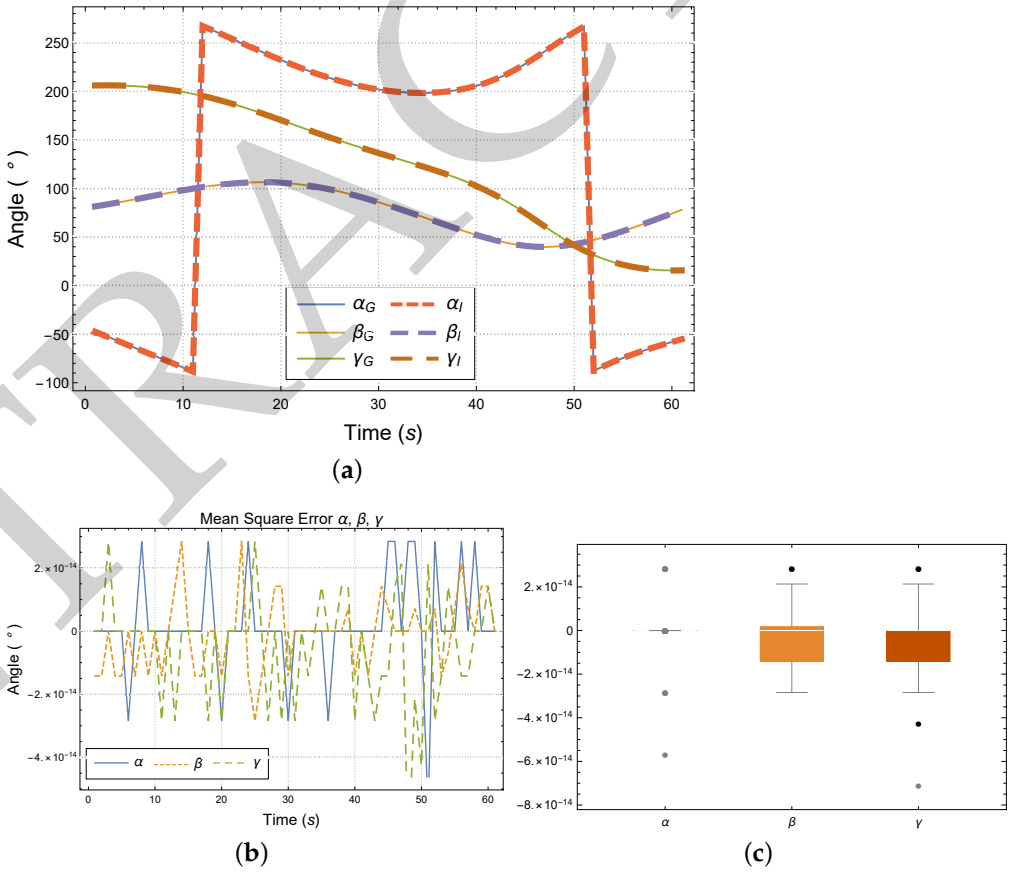


Figure 6. A comparison of the mathematical models of the orientation analysis. (**a**) Comparison of the orientation (α, β, γ) between CAD mechanical design and orientations equations. (**b**) Mean Square Error of the orientation. (**c**) Box plot of the orientation.

Table 8 shows the values of the Mean Square Error and Standard Error of the orientation. In conclusion, the equations of the orientation of the upper-limb exoskeleton are correct.

RETRACTED

Table 8. Mean Squared Error (MSE) and Standard Error (SE) of the Orientation.

Angle	α	β	γ
MSE	1.86372×10^{-15}	-9.31859×10^{-16}	-5.47467×10^{-15}
SE	1.9786×10^{-15}	1.443×10^{-15}	2.26158×10^{-15}

3. Inverse Kinematics of the Upper-Limb Exoskeleton

The comparison of inverse kinematics is developed by inverse kinematics equations and starting angles. To validate the equations of the angles of the inverse kinematics, the Equations (12)–(14) of the forward kinematics and Equations (29)–(31) of the orientation are used to validate. Substituting the values of Table 6, which shows the starting angles for the inverse kinematics, the values of forward kinematics and orientation are obtained. Replacing these values into Equations (39)–(42) of the inverse kinematics verifies that the starting angles and angles values of the inverse kinematics are identical. Furthermore, Figure 7a shows a graphical comparison between the starting angles, which are shown in Table 6 and the angles obtained by the inverse kinematics. Figure 7b shows the Mean Square Error of the angles of the inverse kinematics are approximately equal to zero. Finally, Figure 7c shows the box plot representation of inverse kinematics.

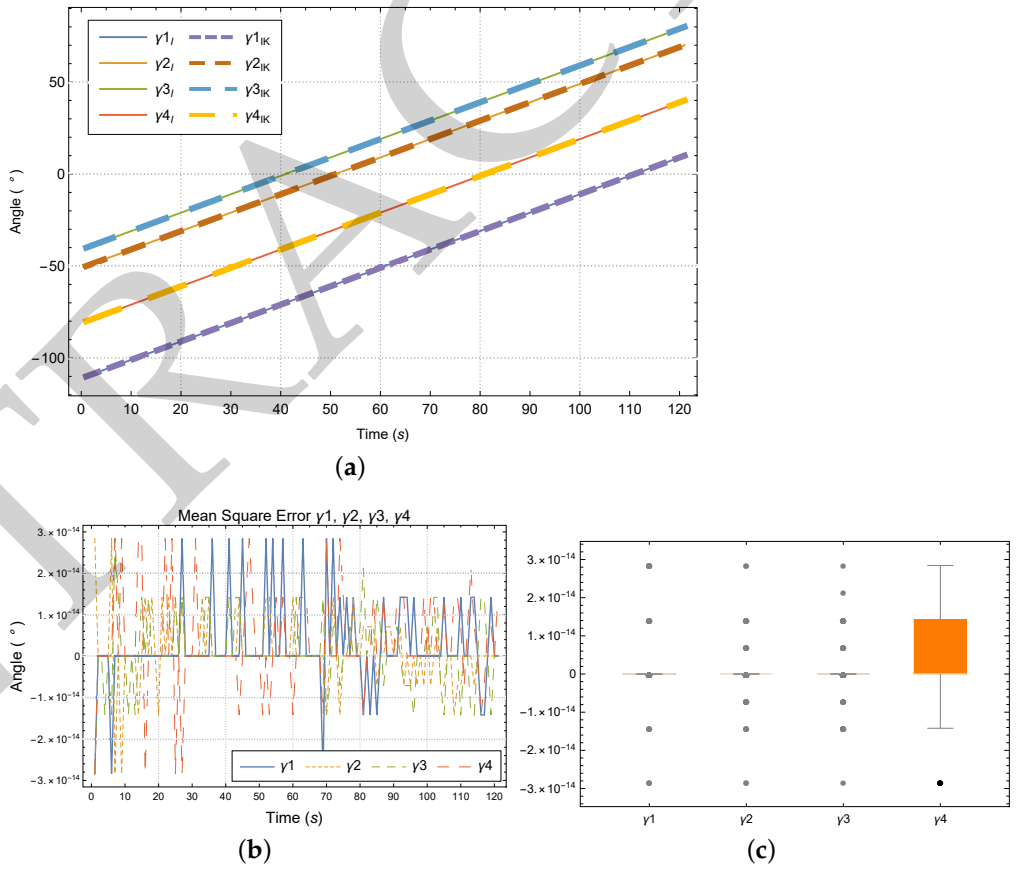


Figure 7. A comparison of the mathematical models of the inverse kinematics. (**a**) Comparison of the inverse kinematics (γ_1, γ_2, γ_3, γ_4) between CAD mechanical design and inverse kinematics equations. (**b**) Mean Square Error of the inverse kinematics. (**c**) Box plot of the inverse kinematics.

Table 9 shows the values of the Mean Square Error and Standard Error of the inverse kinematics. In a conclusion, the inverse kinematics equations are correct.

RETRACTED

Table 9. Mean Squared Error (MSE) and Standard Error (SE) of inverse kinematics.

Angle	γ_1	γ_2	γ_3	γ_4
MSE	2.58379×10^{-15}	9.39561×10^{-16}	9.39561×10^{-16}	3.28846×10^{-15}
SE	9.58096×10^{-16}	7.40929×10^{-16}	7.59468×10^{-16}	1.05826×10^{-15}

3.1.2. Second Numerical Analysis for the Angle Set

This comparison is developed by using a CAD upper-limb exoskeleton to analyze the trajectory of a point of a mechanical model of the system. The forward kinematics equations will be validated by using Table 10, which shows a set of values or configuration obtained from the CAD design, so a study of the movement was performed to validate the values. During the simulation, the mechanism is subjected to angular displacements in the rotation axes from a controlled position, beginning at time t = 0 s with an angular position where the four angles start at $-120°$, $-70°$, $-60°$, $-100°$; and, the ending position at time t = 60 s with an final angular position ends at 35°, 75°, 85°, 45°. This angular position change is applied at a constant rate for every joint in both CAD and mathematical model simulation. These configurations of angles are used as starting angular positions for the numerical examples.

Table 10. Starting angular position for the numerical examples—Second Case.

Angle	γ_1	γ_2	γ_3	γ_4
Range	$[-120°, 35°]$	$[-70°, 75°]$	$[-60°, 85°]$	$[-100°, 45°]$

1. Forward Kinematics of the Upper-Limb Exoskeleton

The position vector $P \in \mathbb{R}^{3x1}$ of the forward kinematics is obtained by Tables 3–6 and Equations (12)–(14). Using the equations of forward kinematics, the values of the final position are obtained for the angles that are defined in Table 10. When comparing to the values of the end position by the CAD mechanical model, both of the positions are identical. Figure 8a shows the graphical comparison of the final position between forward equations and CAD mechanical design. Furthermore, Figure 8b shows the Mean Square Error of the final position that is obtained between the CAD mechanical and forward kinematics. Finally, Figure 8c shows the box plot representation of forward kinematics.

Table 11 shows the Mean Squared Error and Standard Error of the resulting trajectories of the position. The results are approximately equal to zero, so the forward equations kinematics are correct.

Table 11. Mean Squared Error (MSE) and Standard Error (SE) of the Forward Kinematics—Second Case.

Position	P_X **(mm)**	P_Y **(mm)**	P_Z **(mm)**
MSE	-4.06399×10^{-5}	-7.6764×10^{-7}	-2.32297×10^{-5}
SE	3.2964×10^{-6}	4.76053×10^{-6}	4.20971×10^{-6}

RETRACTED

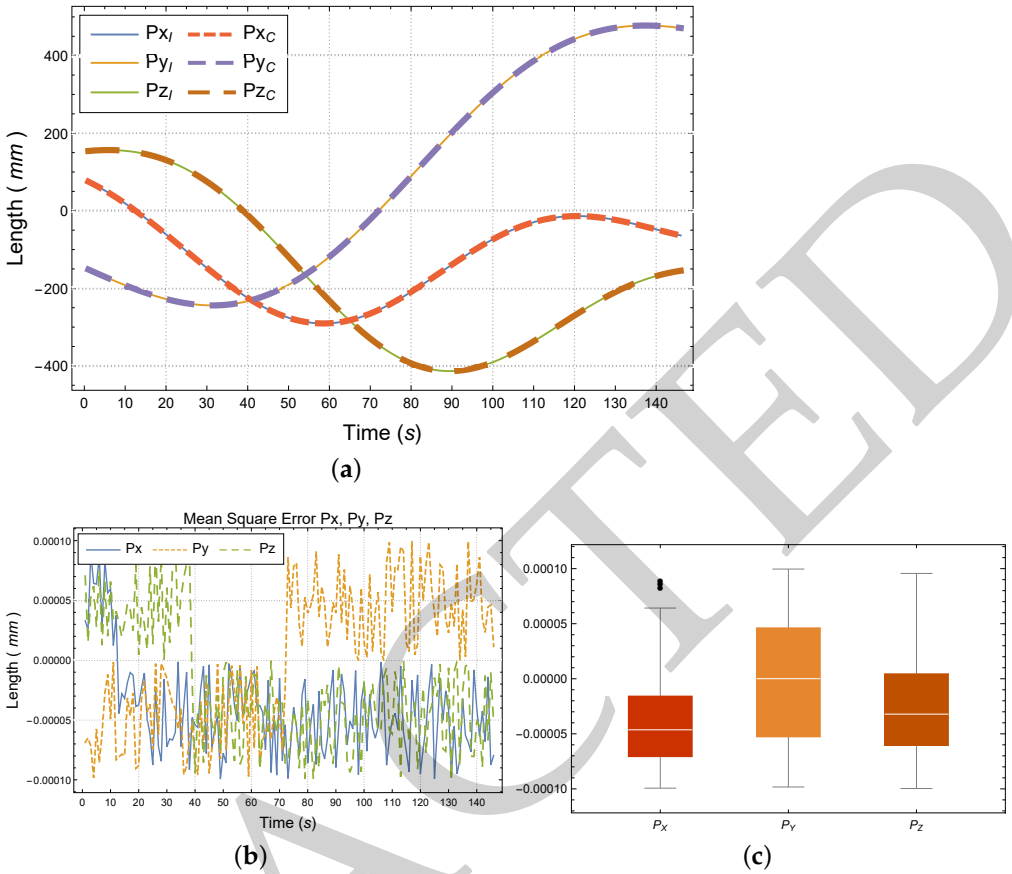


Figure 8. A comparison of the mathematical models of the forward kinematics. (**a**) Comparison of the position (P_X, P_Y, P_Z) between CAD mechanical design and forward kinematics equations. (**b**) Mean Square Error of the forward kinematics. (**c**) Box plot of the forward kinematics.

2. Orientation of the Upper-Limb Exoskeleton

The comparison of the orientation is developed by rotation general equation and orientation equations. Using Table 10 to validate the orientations equations by numerical examples are obtained the values of α, β, γ. Substituting the values of the Table 10 in Equations (29)–(31) are obtained the values of α, β, and γ by orientation equations. Validating the orientation parameters, the general equation of rotation $R_i(\alpha, \beta, \gamma) \in \mathbb{R}^{3\times3}$ in Equation (25) was used to compare both values of the angles. Comparing the results that were obtained using the equations of orientation and the general equation of rotation, the values obtained (α, β, γ) are identical. Furthermore, Figure 9a shows a graphical comparison using a set of values of the four angles that are represented in Table 10. Figure 9b shows the Mean Square Error of the angle's orientation at approximately zero. Finally, Figure 9c shows the box plot representation of orientation.

Table 12 shows the values of the Mean Square Error and Standard Error of the orientation. In conclusion, the equations of the orientation of the upper-limb exoskeleton are correct.

Table 12. Mean Squared Error (MSE) and Standard Error (SE) of the Orientation—Second Case.

Angle	α	β	γ
MSE	-1.21668×10^{-15}	8.27344×10^{-16}	-2.43337×10^{-15}
SE	1.7146×10^{-15}	1.23449×10^{-15}	1.87673×10^{-15}

RETRACTED

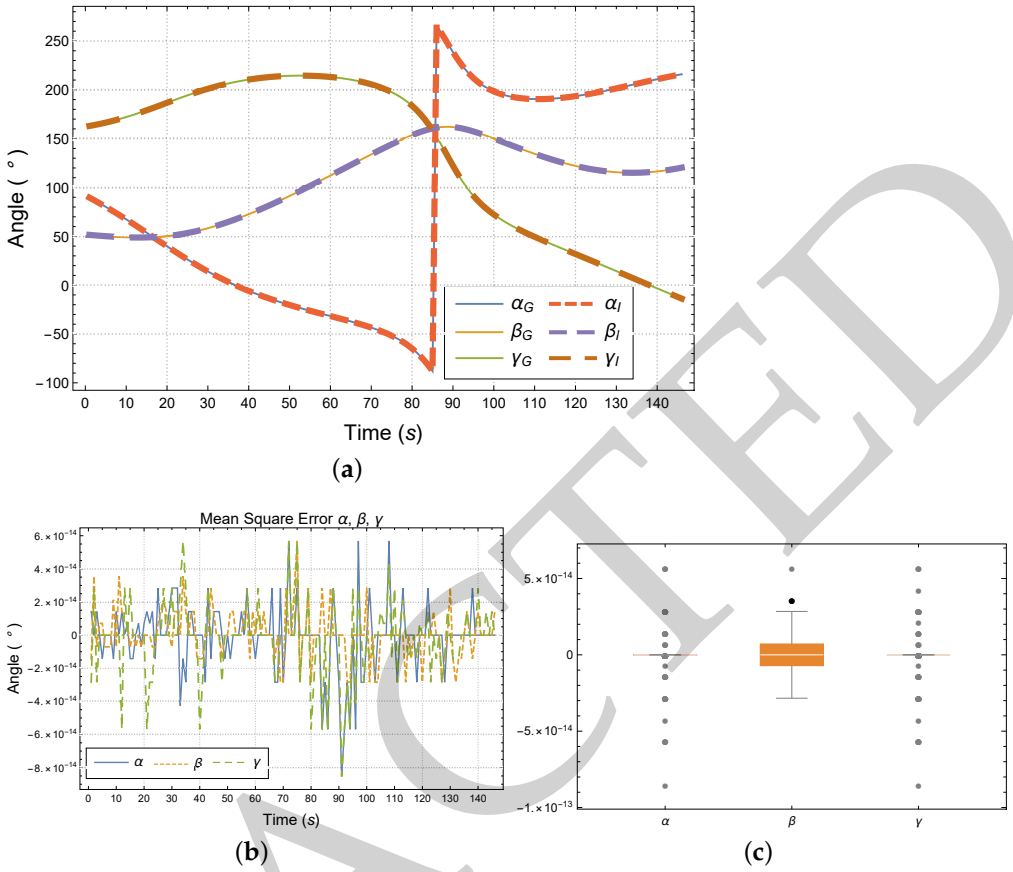


Figure 9. A comparison of the mathematical models of the orientation analysis. (**a**) Comparison of the orientation (α, β, γ) between CAD mechanical design and orientations equations. (**b**) Mean Square Error of the orientation. (**c**) Box plot of the orientation.

3. Inverse Kinematics of the Upper-Limb Exoskeleton

The comparison of inverse kinematics is developed by inverse kinematics equations and starting angles. To validate the equations of the angles of the inverse kinematics, the Equations (12)–(14) of the forward kinematics and Equations (29)–(31) of the orientation are used for validation. Substituting the values of Table 10, which shows the starting angles for the inverse kinematics, the values of forward kinematics and orientation are obtained. Replacing these values into Equations (39)–(42) of the inverse kinematics verifies that the starting angles and angles values of the inverse kinematics are identical. Furthermore, Figure 10a shows a graphical comparison between the starting angles, which are shown in Table 10 and the angles obtained by the inverse kinematics. Figure 10b shows that the Mean Square Error of the angles of the inverse kinematics are approximately equal to zero. Finally, Figure 10c shows the box plot representation of inverse kinematics.

Table 13 shows the values of the Mean Square Error and Standard Error of the inverse kinematics. In conclusion, the inverse kinematics equations are correct.

Table 13. Mean Squared Error (MSE) and Standard Error (SE) of inverse kinematics—Second Case.

Angle	γ_1	γ_2	γ_3	γ_4
MSE	2.62803×10^{-15}	1.31402×10^{-16}	2.33603×10^{-15}	3.01737×10^{-15}
SE	7.47073×10^{-16}	6.69602×10^{-16}	7.96800×10^{-16}	1.00281×10^{-15}

RETRACTED

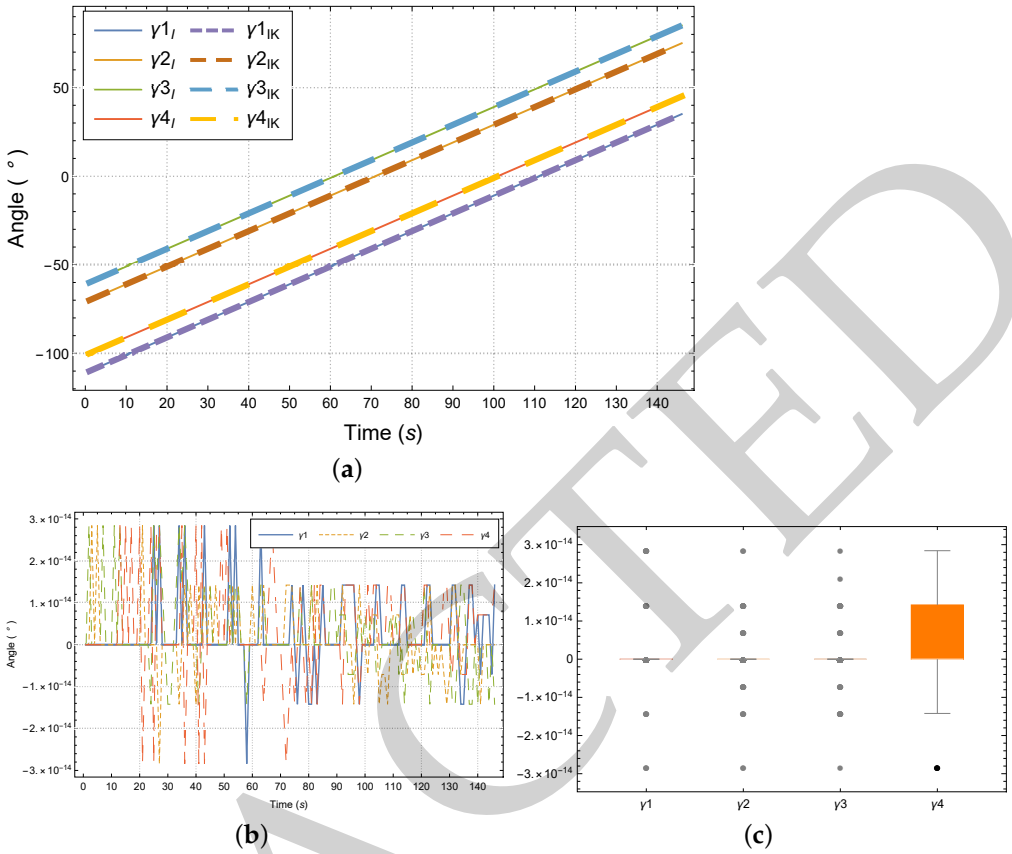


Figure 10. A comparison of the mathematical models of the inverse kinematics. (**a**) Comparison of the inverse kinematics (γ_1, γ_2, γ_3, γ_4) between CAD mechanical design and inverse kinematics equations. (**b**) Mean Square Error of the inverse kinematics. (**c**) Box plot of the inverse kinematics.

The following section will present the workspace of the upper-limb exoskeleton, which will be used for the synchronization task.

3.1.3. Workspace of the Upper-Limb Exoskeleton Using Inverse Kinematics

The range of motion of each angle of the inverse kinematics of Table 2 is used to obtain the generation of the point cloud of the workspace of the upper-limb exoskeleton. Movements are limited because some positions and orientations are not used for synchronization. Figure 11 presents four equally spaced views of the exoskeleton placed on the body generating the anatomical workspace.

The 3D model estimation from the data was exported to an STL format file to obtain the volume of the workspace. The representation of the workspace refers to the final positions that the end effector of the upper-limb exoskeleton performed by means of an information acquisition system that is known as Vicon. The point cloud was extracted for data manipulation, in this way be able to obtain a volume and visualize the ranges of movements that the exoskeleton could perform. In Figure 12, a sample of the workspace of the upper-limb exoskeleton that was used for the synchronization was extracted.

RETRACTED

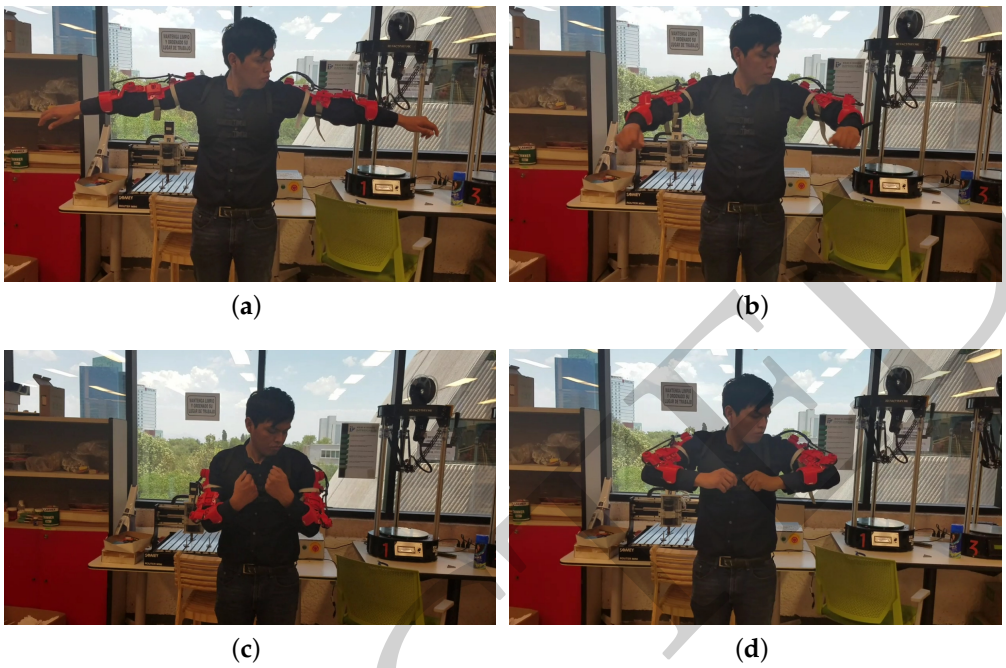


Figure 11. Experimental human workspace for the upper limb. (**a**) Movement of the first joint (γ_1) between the ranges of $< -180°, 180° >$. (**b**) Movement of the second joint (γ_2) between the ranges of $< -90°, 90° >$. (**c**) Movement of the third joint (γ_3) between the ranges of $< -90°, 90° >$. (**d**) Movement of the fourth joint (γ_4) between the ranges of $< -180°, 180° >$.

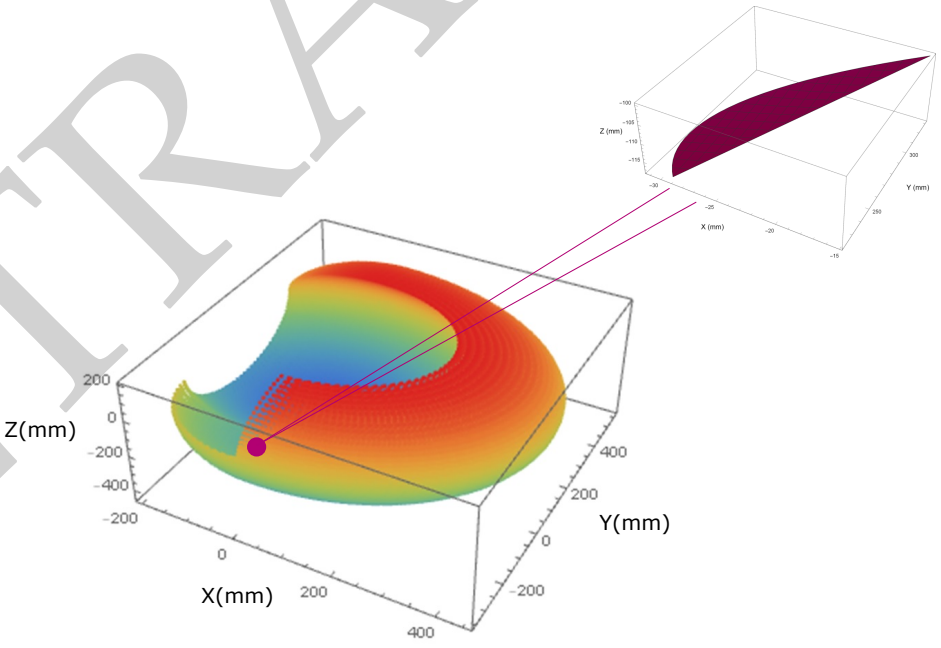
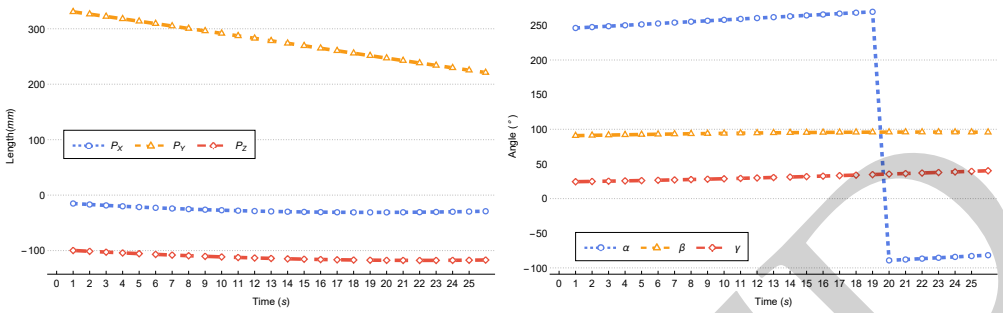


Figure 12. Workspace of the upper-limb exoskeleton.

3.2. Simulation of the Synchronization between Upper-Limb Exoskeleton and Virtual Object

A sample of the workspace (see Figure 12) is taken to perform an analysis kinematic and verify whether both of the proposed systems could be synchronized. Figure 13 shows the position and orientation values of the sample of the upper-limb exoskeleton workspace to be evaluated.

RETRACTED



(**a**) (**b**)

Figure 13. A sample of workspace. (**a**) Position (P_X, P_Y, P_Z). (**b**) Orientation (α, β, γ).

3.2.1. Upper-Limb Exoskeleton Simulation

The purpose of the upper-limb exoskeleton simulation is to obtain the position and orientation with the configuration of angles for their four joints, in this way, it is guaranteed that the upper-limb exoskeleton with its respective angles reaches the appropriate position and orientation. Thus, improper movement is prevented, even though the position and orientation are correct. The inverse kinematics are used to avoid the wrong angle configurations that cause inadequate movement. The mathematical model ensures that there is only one configuration of angles in the four joints for a given position and orientation.

Given position and orientation values in the Figure 13, it is proceeded to obtain the four angles of the upper-limb exoskeleton through the mathematical models of the inverse kinematics using Equations (39)–(42). Substituting the values into the equations mentioned, the four angles are obtained and represented in Figure 14.

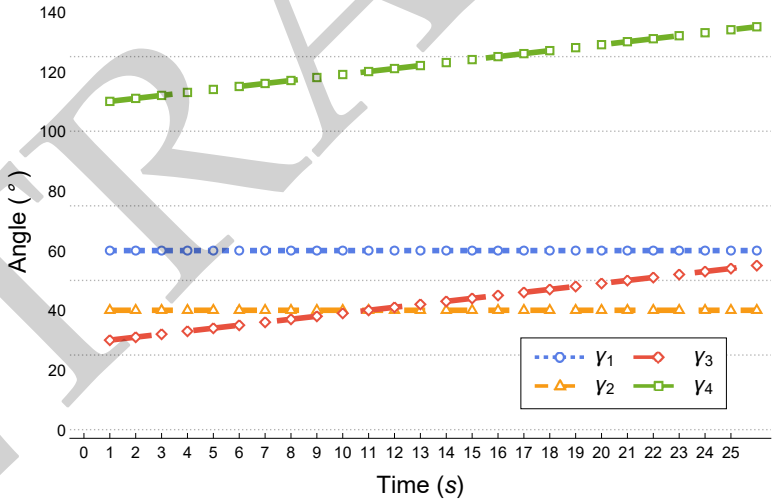


Figure 14. Inverse kinematics angles γ_1, γ_2, γ_3, γ_4.

Figure 14 obtains the numerical values of the four angles of the inverse kinematics. Table 14 shows the angles configuration of the four joints of the upper-limb exoskeleton for a given position and orientation.

Table 14. Inverse kinematics angles.

Angle	γ_1	γ_2	γ_3	γ_4
Value	60°	40°	[30°, 55°]	[110°, 135°]

The numerical values of the position and orientation are obtained by using the configuration of the angle of the upper-limb exoskeleton, which is shown in Table 14. Substituting

RETRACTED

the values into Equations (12)–(14) of the forward kinematics and Equations (29)–(31) of the orientation are calculated. Figure 15a shows a graphical comparison between the initial values of the position of the sample and the values of the forward kinematics equations. Figure 15b shows a graphical comparison between the initial values of the orientation of the sample and the values of the orientation equations.

3.2.2. Virtual Object Simulation

The purpose of virtual object simulation is to obtain the final position and orientation by using homogeneous transformation matrices. Given the position and orientation of the workspace sample, it is proceeded to obtain the position and orientation of the virtual object using Equation (45). Furthermore, the vector $\vec{e}_R$ is a constant because it is a fixed value that is obtained by anatomical measurements. Table 15 establishes the position vector $\vec{e}_R$ of the VR glasses.

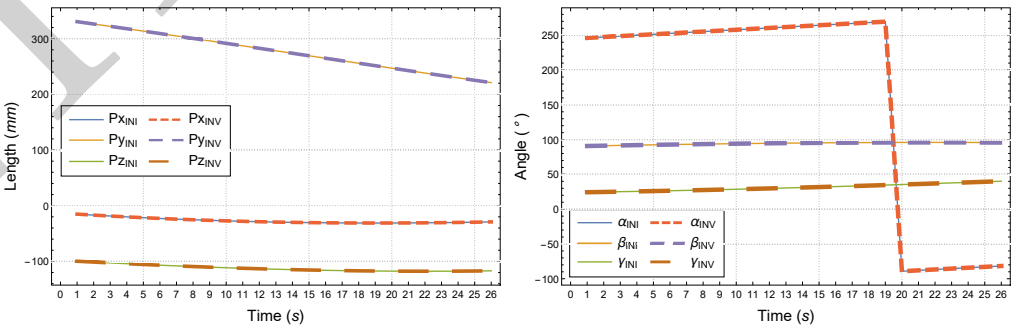
Table 15. Parameters of the VR glasses position's.

Parameter	E_{Rx}	E_{Ry}	E_{Rz}
Value (mm)	0	100	270

The virtual object simulation uses the values that were established in Figure 13 to obtain the matrices E_S and E_M values. Substituting the values of Figure 13 and Table 15 into Equation (45) to obtain the position and orientation of the virtual object. Figure 15a shows a graphical comparison between the initial values of the position of the sample and the values of the object virtual equations. Figure 15b shows a graphical comparison between the initial values of the orientation of the sample and the values of the object virtual equations.

3.2.3. Synchronization Simulation between the Upper-Limb Exoskeleton and Virtual Object

The purpose of the synchronization simulation is to obtain the position and orientation values of the upper-limb exoskeleton (E_T) for L_1 and the virtual object (E_M) for L_2. Synchronization will be performed if Equation (7) is fulfilled. The first opened-loop of the upper-limb exoskeleton (L_1) and the second opened-loop of the virtual object (L_2 was previously analyzed by simulations where the position and orientation graphs were obtained.



(**a**) (**b**)

Figure 15. Position and orientation synchronization simulations between an upper-limb exoskeleton and virtual object. (**a**) Comparison between initial position and forward kinematics equations by using inverse kinematics (P_X, P_Y, P_Z). (**b**) A comparison between the initial orientation and orientation equations using inverse kinematics (α, β, γ).

The Mean Square Error was obtained using the opened-loop graphs. Figure 16a shows a graphical of the Mean Square Error of the position between the upper-limb exoskeleton and virtual object. Figure 16b shows a graphical of the Mean Square Error of the orientation between the upper-limb exoskeleton and the virtual object. Figure 16c shows a graphical of

RETRACTED

the box plot of the position synchronization. Figure 16d shows a graphical of the box plot of the orientation synchronization.

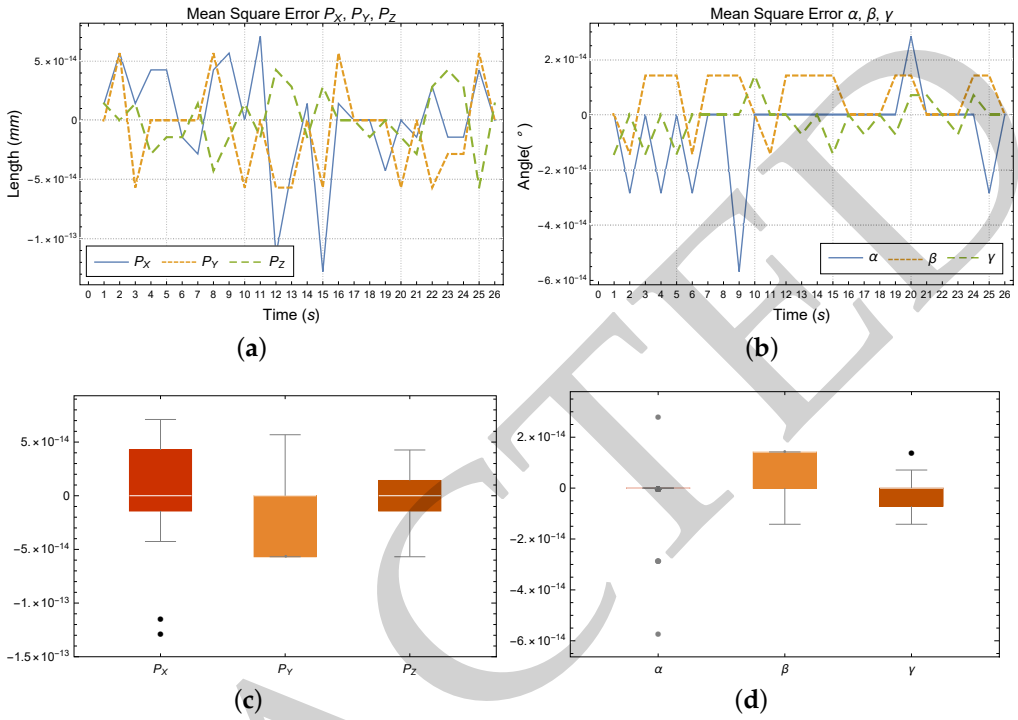


Figure 16. Simulations of position and orientation error synchronization between an upper-limb exoskeleton and virtual object. (**a**) Mean Square Error of the position synchronization (P_X, P_Y, P_Z). (**b**) Mean Square Error of the orientation synchronization (α, β, γ). (**c**) Box plot of the position synchronization (P_X, P_Y, P_Z). (**d**) Box plot of the orientation synchronization (α, β, γ).

The Mean Square Error and Standard Error values of the position synchronization are shown in Table 16. The error obtained to give a value approximately to zero, so the position synchronization is fulfilled.

Table 16. Mean Squared Error (MSE) and Standard Error (SE) of Position.

Position	P_X	P_Y	P_Z
MSE	1.09314×10^{-15}	-8.74514×10^{-15}	5.46571×10^{-16}
SE	9.1902×10^{-15}	7.3558×10^{-15}	4.95303×10^{-15}

Furthermore, Table 17 shows the Mean Square Error and Standard Error values of the orientation synchronization. The error obtained to give a value approximately to zero, so the position synchronization is fulfilled.

Table 17. Mean Squared Error (MSE) and Standard Error (SE) of Orientation.

Angle	α	β	γ
MSE	-5.46571×10^{-15}	6.01228×10^{-15}	-1.913×10^{-15}
SE	3.16068×10^{-15}	1.95853×10^{-15}	1.3967×10^{-15}

In conclusion, the proposed system gives a value of approximately zero, so the upper-limb exoskeleton and the virtual object reach the same position and orientation. Therefore, the synchronization between both of the proposed systems was fulfilled.

RETRACTED

4. Conclusions

Kinematic analysis plays an important role in achieving synchronization between the upper-limb exoskeleton and the virtual object projected by immersive virtual reality glasses. The objective of inverse kinematics is to determine a set of joint angles given a known pose of the end effector, which is, to obtain a unique angle configuration for a suitable position and orientation. In this way, it is avoided to have an inadequate joint configuration in the exoskeleton of the upper-limb. The use of inverse kinematics is very important in the practical handling of robotic manipulators, such as the upper-limb exoskeleton, since they work with objects in each joint space, so determining the angles of the joints is important. Besides, it is not enough with only the articular angles, but the orientation angles must be complemented, because it is not only to achieve the articular position, but to do it with the proper orientation.

To achieve synchronization between both systems, inverse kinematics and orientation analysis must be properly applied to be later validated through simulation through numerical examples for its correct functionality. Finding the mathematical models of the angles of the inverse kinematics is not as "simple" as finding a solution of the position of the direct kinematics for serial robots, such as exoskeletons. The mathematical models of the kinematic analysis and orientation were obtained using Pieper's methods and Euler's angles, respectively. Additionally, kinematic analysis of the virtual object was performed using Euler angles to obtain the position and orientation. The workspace was obtained using the delimited range of motion of the four joints of the exoskeleton of the upper-limb that was taken as a prototype. After the analysis, the MSE obtained for each angle was approximately zero, so the mathematical models of the angles of the inverse kinematics and orientation were correct. To corroborate the equations, numerical examples were performed that validated the kinematic equations of the exoskeleton of the upper-limb and the virtual object. For this, a sample of the upper-limb exoskeleton workspace was used to validate the position and orientation in the simulation.

The synchronization was performed using the position values of the exoskeleton of the upper-limb and the virtual object, resulting in the proposed systems reaching the same point in position and orientation, thereby achieving synchronization of the exoskeleton of the upper-limb and the virtual object.

The application of the proposed synchronization between an upper-limb exoskeleton and a virtual object projected by virtual reality will allow the movements to be performed in rehabilitation therapies to be precise and correct. To use the obtained results, an upper-limb motor training system in virtual reality has been developed and the exoskeleton has been instrumented with sensors to obtain positions and orientations. In this way, new tests can be performed to verify that the kinematic analyses obtained in this work are correct and they can be applied in the performance tests in a real environment.

Finally, a future line of intervention is to include these motor training systems with the upper-limb exoskeleton and virtual reality as a complementary aid to the rehabilitation routines performed by the responsible medical personnel. Additionally, it is expected to have an acceptable efficacy percentage to be able to perform more functional tests in a real environment. Consequently, it is desired to intervene in the improvement of the recovery process of end-users while using these technological tools. Depending on the results that were obtained in a real environment, it plans to extend and work with a lower-limb exoskeleton to have a full-body exoskeleton to be used in rehabilitation therapies for the different disabilities of end-users.

Author Contributions: Conceptualization, D.H.; methodology, D.H. and A.V.-M.; software, D.H.; resources, D.H. and A.V.-M.; writing—original draft preparation, D.H.; writing—review and editing, D.H., A.V.-M. and R.R.-M.; supervision, A.V.-M. and R.R.-M. All authors have read and agreed to the published version of the manuscript.

Funding: This work was supported by Consejo Nacional de Ciencia y Tecnología (CONACYT), Tecnologico de Monterrey and the National Robotics Laboratory at Tecnologico de Monterrey.

RETRACTED

Data Availability Statement: The data that support the findings of this study are available from the corresponding author upon reasonable request.

Conflicts of Interest: The authors declare no conflict of interest

References

1. Kiguchi, K.; Iwami, K.; Yasuda, M.; Watanabe, K.; Fukuda, T. An exoskeletal robot for human shoulder joint motion assist. *IEEE/ASME Trans. Mechatron.* **2003**, *8*, 125–135. [CrossRef]
2. Cloud, W. *Man Amplifiers: Machines That Let You Carry a Ton*; Popular Science: Harlan, IA, USA, 1965; pp. 70–73.
3. Kazerooni, H. The human power amplifier technology at the University of California, Berkeley. *Robot. Auton. Syst.* **1996**, *19*, 179–187. [CrossRef]
4. Gull, M.A.; Bai, S.; Bak, T. A review on design of Upper Limb Exoskeleton. *Robotics* **2020**, *9*, 16. [CrossRef]
5. Nguiadem, C.; Raison, M.; Achiche, S. Motion planning of Upper-Limb exoskeleton robots: A review. *Appl. Sci.* **2020**, *10*, 7626. [CrossRef]
6. Piña-Martínez, E.; Roberts, R.; Leal-Merlo, S.; Rodriguez-Leal, E. Vision System-Based Design and Assessment of a Novel Shoulder Joint Mechanism for an Enhanced Workspace Upper Limb Exoskeleton. *Appl. Bionics Biomech.* **2018**, *2018*, 6019381. [CrossRef] [PubMed]
7. Lo, H.S.; Xie, S.Q. Exoskeleton robots for upper-limb rehabilitation: State of the art and future prospects. *Med. Eng. Phys.* **2012**, *34*, 261–368. [CrossRef] [PubMed]
8. Kim, B.; Deshpande, A.D. An upper-body rehabilitation exoskeleton harmony with an anatomical shoulder mechanism: Design, modeling, control, and performance evaluation. *Int. J. Robot. Res.* **2017**, *36*, 414–435. [CrossRef]
9. Jayaraman, A.; Marinov, B.; Singh, Y.; Burt, S.; Rymer, W.Z. Current Evidence for Use of Robotic Exoskeletons in Rehabilitation. In *Wearable Robotics*; Elsevier: Amsterdam, The Netherlands, 2020; pp. 301–310.
10. Prange, G.; Kottink, A.; Buurke, J.H.; Eckhardt, M.; van Keulen-Rouweler, B.; Ribbers, G.; Rietman, J. The effect of arm support combined with rehabilitation games on upper-extremity function in subacute stroke: A randomized controlled trial. *Neurorehabil. Neural Repair* **2015**, *29*, 174–182. [CrossRef]
11. Bertani, R.; Melegari, C.; De Cola, M.C.; Bramanti, A.; Bramanti, P.; Calabrò, R.S. Effects of robot-assisted upper limb rehabilitation in stroke patients: A systematic review with meta-analysis. *Neurol. Sci. Off. J. Ital. Neurol. Soc. Ital. Soc. Clin. Neurophysiol.* **2017**, *38*, 1561–1569. [CrossRef]
12. Franck, J.A. Rehabilitation of Patients with a Moderately to Severely Affected Arm-Hand in the Sub-Acute Phase after Stroke. Ph.D. Thesis, Maastricht University, Maastricht, The Netherlands, 2020.
13. Peng, L.; Hou, Z.; Peng, L.; Luo, L.; Wang, W. Robot assisted upper limb rehabilitation training and clinical evaluation: Results of a pilot study. In Proceedings of the IEEE International Conference on Robotics and Biomimetics (ROBIO), Macau, Macao, 5–8 December 2017; pp. 2740–2745.
14. Maciejasz, P.; Eschweiler, J.; Gerlach-Hahn, K.; Jansen-Troy, A.; Leonhardt, S. A survey on robotic devices for upper limb rehabilitation. *J. NeuroEng. Rehabil.* **2014**, *11*, 3. [CrossRef]
15. Krishnan, R.; Björsell, N.; Gutierrez-Farewik, E.M.; Smith, C. A survey of human shoulder functional kinematic representations. *Med. Biol. Eng. Comput.* **2019**, *57*, 339–367. [CrossRef] [PubMed]
16. Chen, C.; Lien, W.; Chen, C.; Wu, Y. Implementation of an Upper-Limb Exoskeleton Robot Driven by Pneumatic Muscle Actuators for Rehabilitation. *Actuators* **2020**, *9*, 106. [CrossRef]
17. Głowinski, S.; Krzyzynski, T.; Pecolt, S.; Maciejewsk, I. Design of motion trajectory of an arm exoskeleton. *Arch. Appl. Mech.* **2015**, *85*, 75–87. [CrossRef]
18. Zhang, L.; Li, L.; Chen, Z.; Song, D. Prototype design, modeling, and experimental research of a novel lower limb powered exoskeleton. *Proc. Inst. Mech. Eng. Part C J. Mech. Eng. Sci.* **2017**, *231*, 3766–3779. [CrossRef]
19. Xiao, F.; Gao, Y.; Wang, Y.; Zhu, Y.; Zhao, J. Design and evaluation of a 7-DOF cable-driven upper limb exoskeleton. *J. Mech. Sci. Technol.* **2018**, *32*, 855–864. [CrossRef]
20. Clerval, J.; Lacombe, R.; Adolphe, M.; Zagrodny, B.; Kirchof, Z. Center of mass of human's body segments. *Mech. Mech. Eng.* **2017**, *21*, 485–497.
21. Do Tran, V.; Dario, P.; Mazzoleni, S. Kinematic measures for upper limb robot-assisted therapy following stroke and correlations with clinical outcome measures: A review. *Med. Eng. Phys.* **2018**, *53*, 13–31. [CrossRef]
22. Lupparielli, L.; Faiella, G.; Macias, P.; Cesarelli, M.; Nespoli, M.; Clemente, F. Novel kinematics indexes for the upper limb reaching movements evaluation with robotic exoskeleton. In Proceedings of the 2020 IEEE International Symposium on Medical Measurements and Applications (MeMeA), Bari, Italy, 1 June–1 July 2020; pp. 1–5.
23. Schwarz, A.; Kanzler, C.M.; Lambercy, O.; Luft, A.R.; Veerbeek, J.M. Systematic review on kinematic assessments of upper limb movements after stroke. *Stroke* **2019**, *50*, 718–727. [CrossRef]
24. Hall, P.T.; Crouch, D.L. Effect of continuous, mechanically passive, anti-gravity assistance on kinematics and muscle activity during dynamic shoulder elevation. *J. Biomech.* **2020**, *103*, 109685. [CrossRef] [PubMed]
25. De Lima Boarati, E.; Hotta, G.H.; McQuade, K.J.; de Oliveira, A.S. Acute effect of flexible bar exercise on scapulothoracic muscles activation, on isometric shoulder abduction force and proprioception of the shoulder of individuals with and without subacromial pain syndrome. *Clin. Biomech.* **2020**, *72*, 77–83. [CrossRef] [PubMed]

PREPRINTED

26. Delgado, P.; Alekhya, S.; Majidirad, A.; Hakansson, N.; Desai, J.; Yihun, Y. Shoulder Kinematics Assessment towards Exoskeleton Development. *Appl. Sci.* **2020**, *10*, 6336. [CrossRef]
27. MajidiRad, A.; Yihun, Y.S. Upper Limb Rehabilitation and Mobility Assistance Using Robotic Devices: A Review. In Proceedings of the ASME 2019 International Design Engineering Technical Conferences and Computers and Information in Engineering Conference, American Society of Mechanical Engineers Digital Collection, Anaheim, CA, USA, 18–21 August 2019.
28. Brihmat, N.; Loubinoux, I.; Castel-Lacanal, E.; Marque, P.; Gasqcorresponding, D. Kinematic parameters obtained with the ArmeoSpring for upper-limb assessment after stroke: A reliability and learning effect study for guiding parameter use. *J. NeuroEng. Rehabil.* **2020**, *17*, 130. [CrossRef] [PubMed]
29. Wang, C.; Peng, L.; Hou, Z. Kinematic Redundancy Analysis during Goal-Directed Motion for Trajectory Planning of an Upper-Limb Exoskeleton Robot. In Proceedings of the 41st Annual International Conference of the IEEE Engineering in Medicine and Biology Society (EMBC), Berlin, Germany, 23–27 July 2019; pp. 5251–5255.
30. Wang, K.; Sun, M.; Xia, R.; Mao, Z. Human-robot symbiosis framework on exoskeleton devices. In Proceedings of the 2016 IEEE International Conference on Industrial Technology (ICIT), Taipei, Taiwan, 14–17 March 2016; pp. 1500–1506.
31. Oluwatosin, M.; Djouani, K.; Hamam, Y. Interaction Control for Human-Exoskeletons. *J. Control Sci. Eng.* **2020**, *2020*, 8472510.
32. Guo, J.; Li, P.; Guo, S. Design and Analysis of a Wearable Exoskeleton Upper Limb Rehabilitation Robot. In Proceedings of the 2020 IEEE International Conference on Mechatronics and Automation (ICMA), Beijing, China, 13–16 October 2020; pp. 1564–1569.
33. Wang, L.; Hu, X. Design kinematics simulation and dynamic analysis of the wearable upper-limb rehabilitation robot. *Beijing Biomed. Eng.* **2017**, *36*.
34. Mândru, D.; Tătar, O.; Noveanu, S.; Ianoşi-Andreeva-Dimitrova, A. Design and Modelling 4 DOFs Upper Limb Exoskeleton. *Appl. Mech. Mater.* **2016**, *823*, 107–112. [CrossRef]
35. López-Méndez, S.; Martínez-Tejada, H.; Valencia-García, M. Development of an armored upper limb exoskeleton. *Rev. Fac. Ing. Univ. Antioq.* **2020**, *95*, 109–117. [CrossRef]
36. Papaleo, E.; Zollo, L.; Garcia-Aracil, N.; Badesa, F.J.; Morales, R.; Mazzoleni, S.; Sterzi, S.; Guglielmelli, E. Upper-limb kinematic reconstruction during stroke robot-aided therapy. *Med. Biol. Eng. Comput.* **2015**, *53*, 815–828. [CrossRef]
37. Qassim, H.M.; Wan Hasan, W.Z. A Review on Upper Limb Rehabilitation Robots. *Appl. Sci.* **2020**, *10*, 6976. [CrossRef]
38. Oña, E.D.; Garcia-Haro, J.M.; Jardón, A.; Balaguer, C. Robotics in Health Care: Perspectives of Robot-Aided Interventions in Clinical Practice for Rehabilitation of Upper Limbs. *Appl. Sci.* **2019**, *9*, 2586. [CrossRef]
39. Liu, F.; Han, X.; Lin, M.; Wu, X.; Sun, Q.; Song, A. Remote Upper Limb Exoskeleton Rehabilitation Training System Based on Virtual Reality. In Proceedings of the 2019 16th International Conference on Ubiquitous Robots (UR), Jeju, Korea, 24–27 June 2019; pp. 323–327.
40. Cai, H.; Lin, T.; Chen, L.; Weng, H.; Zhu, R.; Chen, Y.; Cai, G. Evaluating the effect of immersive virtual reality technology on gait rehabilitation in stroke patients: A study protocol for a randomized controlled trial. *Trials* **2021**, *22*, 91. [CrossRef]
41. Kim, W.-S.; Cho, S.; Ku, J.; Kim, Y.; Lee, K.; Hwang, H.-J.; Paik, N.-J. Clinical Application of Virtual Reality for Upper Limb Motor Rehabilitation in Stroke: Review of Technologies and Clinical Evidence. *J. Clin. Med.* **2020**, *9*, 3369. [CrossRef] [PubMed]
42. Levin, M.; Demers, M. Motor learning in neurological rehabilitation. *Disabil. Rehabil.* **2020**, 1–9. [CrossRef] [PubMed]
43. Xie, S. Advanced robotics for medical rehabilitation. In *Springer Tracts in Advanced Robotics*; Springer: Berlin/Heidelberg, Germany, 2016.
44. Pieper, D.L.; Roth, B. The Kinematics of Manipulators Under Computer Control. In Proceedings of the II International Congress on the Theory of Machines and Mechanisms, Zakopane, Poland, 23–27 September 1969; Volume 2, pp. 159–169.
45. Shahab, M.; Raisi, M.; Hejrati, M.; Taheri, A.; Meghdari, A. Virtual Reality Robot for Rehabilitation of Children with Cerebral Palsy (CP). In Proceedings of the 2019 7th International Conference on Robotics and Mechatronics (ICRoM), Tehran, Iran, 20–21 November 2019; pp. 63–68.
46. Boone, A.; Wolf, T.; Engsberg, J. Combining Virtual Reality Motor Rehabilitation With Cognitive Strategy Use in Chronic Stroke. *Am. J. Occup. Ther.* **2019**, *73*, 7304345020. [CrossRef]
47. Sucar, L.E.; Orihuela-Espina, F.; Velazquez, R.L.; Reinkensmeyer, D.J.; Leder, R.; Hernández-Franco, J. Gesture therapy: An upper limb virtual reality-based motor rehabilitation platform. *IEEE Trans. Neural Syst. Rehabil. Eng.* **2014**, *22*, 634–643. [CrossRef] [PubMed]
48. Rathinam, C.; Mohan, V.; Peirson, J.; Skinner, J.; Nethaji, K.; Kuhn, I. Effectiveness of virtual reality in the treatment of hand function in children with cerebral palsy: A systematic review. *J. Hand Ther.* **2019**, *32*, 426–434. [CrossRef]
49. Mubin, O.; Alnajjar, F.; Jishtu, N.; Alsinglawi, B.; Al Mahmud, A. Exoskeletons With Virtual Reality, Augmented Reality, and Gamification for Stroke Patients' Rehabilitation: Systematic Review. *JMIR Rehabil. Assist. Technol.* **2019**, *6*, e12010. [CrossRef]
50. Zheng, J.; Shi, P.; Yu, H. A Virtual Reality Rehabilitation Training System Based on Upper Limb Exoskeleton Robot. In Proceedings of the 10th IEEE International Conference on Intelligent Human-Machine Systems and Cybernetics (IHMSC), Hangzhou, China, 25–26 August 2018.
51. Grimm, F.; Naros, G.; Gharabaghi, A. Closed-Loop Task Difficulty Adaptation during Virtual Reality Reach-to-Grasp Training Assisted with an Exoskeleton for Stroke Rehabilitation. *Front. Neurosci.* **2016**, *10*, 518. [CrossRef]
52. Li, J.; Zhao, F.; Li, X.; Li, J. Analysis of robotic workspace based on Monte Carlo method and the posture matrix. In Proceedings of the IEEE International Conference on Control and Robotics Engineering (ICCRE), Singapore, 2–4 April 2016; pp. 1–5.

RETRACTED

53. Pieper, D.L. The Kinematics of Manipulators Under Computer Control. Ph.D. Thesis, Stanford University, Stanford, CA, USA, 1968; p. 157.
54. Lan, Z.; Li, Z.L.; Li, Y. Calculation of Inverse Kinematics Problem of a 5-DOF Rehabilitation Robot for Upper Limb Based on Screw Theory. *Appl. Mech. Mater.* **2010**, *26*, 139–144. [CrossRef]
55. Goldenberg, A.A.; Benhabib, B.; Fenton, R.G. A Complete Generalized Solution to the Inverse Kinematics of Robots. *IEEE J. Robot. Autom.* **1985**, *1*, 14–20. [CrossRef]
56. Loh, B.G.; Rosen, J. Kinematic analysis of 7 degrees of freedom upper-limb exoskeleton robot with tilted shoulder abduction. *Int. J. Precis. Eng. Manuf.* **2013**, *14*, 69–76. [CrossRef]
57. Shah, S.V.; Saha, S.K.; Dutt, J.K. Denavit-Hartenberg Parameterization of Euler Angles. *J. Comput. Nonlinear Dyn.* **2012**, *7*, 021006. [CrossRef]
58. Xu, N.; Peng, X.; Peng, L.; Hou, Z.; Gui, M. Modeling and Kinematics Analysis of a Novel 5-DOF Upper Limb Exoskeleton Rehabilitation Robot. In Proceedings of the 2020 39th Chinese Control Conference (CCC), Shenyang, China, 27–29 July 2020; pp. 1052–1057.
59. Hartenberg, R.S.; Denavit, J. A kinematic notation for lower-pair mechanisms based on matrices. *Trans. ASME. J. Appl. Mech.* **1955**, *22*, 215–221.
60. Lu, J.; Chen, W.; Tomizuka, M. Kinematic Design and Analysis of a 6-DOF Upper Limb Exoskeleton Model for a Brain-Machine Interface Study. *IFAC Proc. Vol.* **2013**, *46*, 293–300. [CrossRef]
61. Zaixiang, P.; Wang, T.; Wang, Z. Design and Analysis of a Wearable Upper Limb Rehabilitation Robot with Characteristics of Tension Mechanism. *Appl. Sci.* **2020**, *10*, 2101.
62. Panich, S. Kinematic Analysis of Exoskeleton Suit for Human Arm. *J. Comput. Sci.* **2010**, *6*, 1272–1275. [CrossRef]
63. Wang, X.; Song, X.; Wang, X.; Liu, P. Kinematics and dynamics analysis of a 3-DOF upper-limb exoskeleton with an internally rotated elbow joint. *Appl. Sci.* **2018**, *8*, 464. [CrossRef]
64. Zeiaee, A.; Soltani-Zarrin, R.; Langari, R.; Tafreshi, R. Design and kinematic analysis of a novel upper limb exoskeleton for rehabilitation of stroke patients. In Proceedings of the 2017 International Conference on Rehabilitation Robotics (ICORR), London, UK, 17–20 July 2017; pp. 759–764.
65. Cortés, C.; de los Reyes-Guzmán, A.; Scorza, D.; Bertelsen, Á.; Carrasco, E.; Gil-Agudo, Á.; Ruiz-Salguero, O.; Flórez, J. Inverse Kinematics for Upper Limb Compound Movement Estimation in Exoskeleton-Assisted Rehabilitation. *BioMed Res. Int.* **2016**, *2016*, 2581924. [CrossRef]
66. Liu, H.; Zhang, Y.; Zhu, S. Novel inverse kinematic approaches for robot manipulators with Pieper-Criterion based geometry. *Int. J. Control Autom. Syst.* **2015**, *13*, 1242–1250. [CrossRef]
67. Gasperina, S.D.; Ghonasgi, K.; de Oliveira, A.C.; Gandolla, M.; Pedrocchi, A.; Deshpande, A. A Novel Inverse Kinematics Method for Upper-Limb Exoskeleton under Joint Coordination Constraints. In Proceedings of the 2020 IEEE/RSJ International Conference on Intelligent Robots and Systems (IROS), Las Vegas, NV, USA, 24 October–24 January 2020; pp. 3404–3409.
68. Alt Murphy, M.; Häger, C.K. Kinematic analysis of the upper extremity after stroke—How far have we reached and what have we grasped? *Phys. Ther. Rev.* **2015**, *20*, 137–156. [CrossRef]

RETRACTED